CrystEngComm

Accepted Manuscript

This article can be cited before page numbers have been issued, to do this please use: A. Shukla, E. Khan, K. Srivastava, K. Sinha, P. Tandon and V. R. Vangala, *CrystEngComm*, 2017, DOI: 10.1039/C7CE00864C.

This is an Accepted Manuscript, which has been through the Royal Society of Chemistry peer review process and has been accepted for publication.

Accepted Manuscripts are published online shortly after acceptance, before technical editing, formatting and proof reading. Using this free service, authors can make their results available to the community, in citable form, before we publish the edited article. We will replace this Accepted Manuscript with the edited and formatted Advance Article as soon as it is available.

You can find more information about Accepted Manuscripts in the author guidelines.

Please note that technical editing may introduce minor changes to the text and/or graphics, which may alter content. The journal's standard Terms & Conditions and the ethical guidelines, outlined in our author and reviewer resource centre, still apply. In no event shall the Royal Society of Chemistry be held responsible for any errors or omissions in this Accepted Manuscript or any consequences arising from the use of any information it contains.

ROYAL SOCIETY OF CHEMISTRY

rsc.li/crystengcomm

View Article Online
DOI: 10.1039/C7CE00864C

CrystEngComm

PAPER

Received 00th January 20xx,
Accepted 00th January 20xx

DOI: 10.1039/x0xx00000x

www.rsc.org/

Study of hydrogen bonding interactions and chemical reactivity analysis of nitrofurantoin–3-aminobenzoic acid cocrystal using quantum chemical and spectroscopic (IR, Raman, ^{13}C SS-NMR) approach

Anuradha Shukla[a], Eram Khan[a], Karnica Srivastava[a], Kirti Sinha[a], Poonam Tandon[a*], Venu R. Vangala[b*]

The investigations of structural reactivity, molecular interactions and vibrational characterization of pharmaceutical drug are helpful to understand their behaviour. The aim of this study is to determine the molecular, electronic and chemical properties of an antibiotic drug, nitrofurantoin (NF), after cocrystallisation with 3-aminorbenzoic acid (3ABA) and to understand as to how those changes lead to variation of properties in the cocrystal, NF-3ABA. NF-3ABA formation is explained by the stabilization *via* hydrogen-bond network between NF and 3ABA molecules. It is thoroughly characterized by IR, Raman and CP-MAS solid-state ^{13}C NMR techniques, along with quantum chemical calculations. The indications of IR, Raman, and ^{13}C NMR showed that imide N–H23 and C12=O of NF interacts with the acid C=O and –OH groups in 3-ABA, respectively. Therefore IR, Raman, and ^{13}C NMR spectra verified the formation of N–H···O and O–H···O hydrogen bonds. To study hydrogen bonding interactions theoretically in NF-3ABA, two functionals; B3LYP and wB97X-D have been used. A comparison is made between the results obtained by B3LYP and those predicted at wB97X-D level. It is found that wB97X-D is best applied density functional theory (DFT) functional to describe the hydrogen bonding interactions. The strength and nature of hydrogen bonding in NF-3ABA have been analysed by quantum theory of atoms in molecules (QTAIM) and natural bond orbital (NBO) analysis. To validate the results obtained by QTAIM theory and to study the long-range forces, such as van der Waals interactions, steric effects in NF-3ABA, the reduced density gradient (RDG) and the isosurface have been plotted using Multiwfn software. QTAIM and isosurface analysis suggested that the hydrogen bonding interactions present in the NF-3ABA are moderate in nature. The calculated HOMO–LUMO energy gap shows that the NF-3ABA is more active than NF and 3ABA. Chemical reactivity descriptors are calculated to understand the various aspects of pharmacological sciences. Chemical reactivity parameters show that the NF-3ABA is more softer and chemically more reactive than NF. The results suggest that cocrystals can be a feasible alternative for positively changing the targetted physicochemical properties of an active pharmaceutical ingredient (API).

I. Introduction

APIs are materials that are most efficiently developed and expressed as solid dosage forms.[1] A significant number of APIs pose poor physical properties during formulation and dosage form development. Cocrystallization is an emerging approach for positively modifying API properties. Pharmaceutical cocrystals are molecular adducts of definite stoichiometry where one component is an API and the other is a counter molecule (co-former) and both components are solids that are crystalline single phase materials.[2] Cocrystals are held together by non-covalent interactions such as hydrogen bonding, π–π-stacking and van der Waal forces within the same crystal lattice.[3,4] Pharmaceutical cocrystals raise important intellectual and physical property issues in the context of drug advancement and delivery.[5] Cocrystals can lead to improvements in physical and chemical stability as well as in mechanical properties by diversifying the number of crystal forms that exist for an API. Cocrystals of an API may show enhanced solubility, bioavailability, stability, and dissolution rates compared to that of pure material.[6]

NF is an antibacterial agent, which is used to treat bacterial infections of the urinary tract (bladder and kidneys). This drug works by interrupting with the bacterial metabolism of carbohydrate, disrupting the formation of the bacterial cell wall and interfering with the production of vital nutrients. This drug has poor water solubility[7] and its dissolution in water is, therefore, the rate-limiting step in its absorption from the gastrointestinal tract.[8] NF presents some bioavailability problems which are strictly related to the crystal size and to the two anhydrate and two monohydrate

[a] *Department of Physics, University of Lucknow, Lucknow 226007, Uttar Pradesh, India*
[b] *Centre for Pharmaceutical Engineering Science, School of Pharmacy and Medical Sciences, University of Bradford, Bradford BD7 1DP, United Kingdom*
† Corresponding authors. *Tel.*: +91 522 2782653; fax: +91 522 2740840
E-mail: poonam_tandon@hotmail.com, poonam_tandon@yahoo.co.uk (P.Tandon)
Tel.: +44 127423 6116, *E-mail*: V.G.R.Vangala@bradford.ac.uk (V. R. Vangala)
Electronic Supplementary Information (ESI) available: See DOI: 10.1039/x0xx00000x

View Article Online
DOI: 10.1039/C7CE00864C

crystalline forms.[9,10] It has been reported that the dissolution rate and bioavailability of NF in commercial tablets decreased upon storage at different relative humidity and elevated temperature.[11] Otsuka and co-workers suggested that the physicochemical stability of NF could be one of the important factors for controlling the bioavailability of commercial preparations.[12]

Research in cocrystals has seen dramatic development in recent years, mostly driven by their pharmaceutical applications where properties such as hardness or tableting, solubility are of paramount importance.[13,14] Recent advancements have indicated a great potential of cocrystals for improving the physicochemical properties of APIs.[15,16] In the recent years, there has been growing interest in the application of *ab initio* calculations to pharmaceutical cocrystals.[17-19] Vibrational spectroscopic investigations combined with quantum chemical calculations have been utilized as one of the most effective tools for providing information about structure, composition, conformation and intra/intermolecular interactions and vibrational analysis of cocrystals.[20,21] Solid state NMR (SS-NMR) spectroscopy has proved to be a remarkable tool to explain the molecular structure and conformation at the molecular level.[22] The isotropic chemical shifts provide the useful information regarding the geometry and reactivity of the atoms within the molecule. The aim of this study is to determine the molecular, electronic and chemical properties of NF after cocrystallisation with 3-aminorbenzoic acid (3ABA) and to understand as to how those changes lead to variation of properties in the cocrystal, NF-3ABA.

In the present study, we have investigated the performance of density functionals, one of which is "standard" functional not including dispersion (B3LYP) while the other has been constructed to account for dispersion (wB97X-D), in reproducing molecular structures. The main differences between B3LYP and wB97X-D are the addition of a semi empirical dispersion term that accounts for the weaker London forces. In this contribution, we have performed detailed computational and vibrational analysis of NF-3ABA and its constituents, NF and 3-ABA employing quantum chemical methods. The solid-state properties of NF-3ABA are mainly governed by the strong intermolecular hydrogen bond forces. DFT has been comprehensively used in the literature to address this type of interactions.[23,24] The effect of intermolecular hydrogen bonding on the infrared (IR), Raman and solid-state NMR spectra of NF-3ABA has been examined by DFT calculations using both B3LYP and wB97X-D functionals with cc-pvTZ basis set. The calculated vibrational spectra are analysed based on the potential energy distribution (PED) analysis. In general, the formation of H-bond can be estimated by the structural parameters (bond length and bond angle), and the strength of the H-bond can also be determined by enlarging or shortening of the H-bond length. However, in many cases, the H-bond interactions are too complex to learn just by the structural parameters. Due to this, the quantum theory of atoms in molecules (QTAIM) and natural bond orbital (NBO) analysis have been used for the analysis of the nature and strength of H-bond.[25] The highest occupied molecular orbital (HOMO) and the lowest unoccupied molecular orbital (LUMO) band gap of NF-3ABA and its constituents have been compared for predicting their stability. Chemical activity has been measured by reactivity descriptors (global and local) and molecular electrostatic potential surface (MEP) for rationalisation and interpretation of diverse aspects of chemical bonding. This study aimed to conceptualize the hydrogen bond formation and its effect on vibrational spectra and natural bond orbitals in NF-3ABA.

II. Experimental details

Bio-Rad, FTS 3000MX FT IR spectrometer was used for transmission infrared spectra of the NF-3ABA, NF and 3ABA. The spectra were collected for 64 scans at 4 cm^{-1} resolution. Typically, ~25 mg of the sample was ground with KBr in an agate mortar and pressed with a steel die into a pellet.

FT-Raman spectrum of the NF-3ABA was recorded on a Bruker IFS 55 EQUINOX with Raman attachment. This instrument uses a 1064 nm Nd–YAG laser line of power 500 mW as the excitation line for recording the Raman spectra in the region 20–3400 cm^{-1}. The spectra were collected for 512 scans at 4 cm^{-1} resolution.

The dispersive Raman microscope used in this study was a JYHoriba LabRAM HR equipped with a confocal microscope, liquid-nitrogen-cooled charge coupled device (CCD) and a multichannel detector (256 pixels × 1024 pixels). The NIR 784.8 nm argon ion laser was selected to excite the Raman scattering. The Raman shift range collected was in the range of 100-1700 cm^{-1} with spectral resolution 1.7-2 cm^{-1}.

Cross-polarization Magic Angle Spinning (CP-MAS) solid state NMR spectra were acquired using a Bruker Avance III HD 400 MHz spectrometer fitted with a 4 mm HX-MAS BB/1H probe head. Samples were packed without further manipulation into 4 mm ceramic spinners. 116 scans were acquired using cross polarization with TOSS spinning sideband suppression. A 1 ms contact time, 120 s recycle delay and a spin rate of 10 kHz was used. Spectral referencing was with respect to an external sample of neat tetramethylsilane (carried out by setting the high-frequency signal from adamantane to 38.5 ppm). All solid-state NMR spectra were obtained at the EPSRC UK National Solid State NMR Service at Durham.

III. Computational details

The electronic structure and optimized geometry of NF-3ABA and its constituents were computed by the DFT method[26] using the Gaussian 09 program[27] package employing cc-pvTZ, correlation consistent polarized valence triple-ζ, basis sets[28,29] and Becke's three parameter (local, nonlocal, Hartree–Fock) hybrid exchange functionals with Lee–Yang–Parr correlation functional (B3LYP)[30,31,32] and wB97X-D functional[33] which uses a version of Grimme's D2 dispersion model. The cc-pVTZ basis set was developed by Dunning and co-workers[34-36] provide a convenient reference set of optimized Gaussian basis sets. A complete set of internal coordinates were defined using Pulay's recommendations[37] for normal mode analysis. The vibrational assignments of the normal modes were suggested based on the PED calculated using the program Gar2Ped.[38] Visualization and confirmation of calculated data were done by using the program GaussView.[39] ^{13}C chemical shifts were calculated for NF-3ABA, NF and 3ABA with GIAO method. Topological properties at bond critical points (BCP) have been studied within the framework of the QTAIM using the AIM2000 package of programs.[40]

View Article Online
DOI: 10.1039/C7CE00864C
CrystEngComm PAPER

IV. Theoretical background

Density functional theory (DFT) calculations yield Raman scattering amplitudes, which cannot be taken directly to be the Raman intensities. Raman scattering cross section, $\partial\sigma_j/\partial\Omega$, which is proportional to Raman intensity can be calculated from the Raman scattering amplitude and predicted wavenumbers for each normal mode using the relationship.[41]

$$\frac{\partial\sigma_j}{\partial\Omega} = \left(\frac{2^4\pi^4}{45}\right)\left(\frac{(\nu_0-\nu_j)^4}{1-\exp\left[\frac{-hc\nu_j}{kT}\right]}\right)\left(\frac{h}{8\pi^2 c\nu_j}\right)S_j$$

S_j and ν_j are the scattering activities and the predicted wavenumbers, respectively of the jth normal mode, ν_0 is the wavenumber of the Raman excitation line and h, c and k are universal constants.

Calculated NMR provide predictions of absolute chemical shift shielding tensors that need to be correlated to conventional σ(TMS) values for comparison with results from typical NMR experiments.[42] First computed isotropic shielding constants(σ) were obtained for each nucleus and these were converted to a chemical shift (δ) value per formula is given below.

$$\delta_i = \sigma_{TMS} - \sigma_i$$

The reference substance was tetramethylsilane (TMS) which is most commonly used reference for ^{13}C spectra.

Mean absolute errors were calculated per formula, for estimating the effect of different functional on calculated NMR spectra:

$$\text{mae} = \frac{\Sigma_n|\,\delta_{exp} - \delta_{cal}|}{n}$$

where δ_{exp} and δ_{cal} represent experimental and calculated chemical shifts, respectively.

By DFT calculation, it is possible to define and clarify the concepts of chemical reactivity. Global DFT descriptors like the chemical potential (μ), hardness (η), softness (s), electronegativity (χ) and the electrophilicity index (ω) investigate the reactivity of the molecule, and this has been established effectively.[43,44] Within the theoretical framework of DFT, global DFT descriptors were calculated as per formula:

$$\mu = -\chi = \frac{1}{2}(E_{HOMO} + E_{LUMO})$$

$$\eta = \frac{1}{2}(E_{LUMO} - E_{HOMO})$$

$$S = \frac{1}{2\eta}$$

$$\omega = \frac{\mu^2}{2\eta}$$

This new reactivity index (ω) measures the stabilization in energy when the system acquires an additional electronic charge (ΔN) from the environment. The maximum electronic charge that the electrophile may accept from the surroundings (ΔN_{max}) may be defined as:

$$\Delta N_{max} = -\frac{\mu}{\eta}$$

The amount of charge transfer between the two molecules A and B could be expressed in terms of electrophilicity charge transfer (ECT)[45] and it is defined as the difference between ΔN_{max} values of interacting molecules. ECT is calculated using equation.

$$ECT = (\Delta N_{max})_A - (\Delta N_{max})_B$$

where

$$(\Delta N_{max})_A = \frac{\mu_A}{\eta_A} \text{ and } (\Delta N_{max})_B = \frac{\mu_B}{\eta_B}$$

Three kinds of fukui functions (FF) around each atomic site, namely, f_k^+, f_k^- and f_k° can be used to describe the electrophilic, nucleophilic and radical reactivity, respectively, which are defined in a finite difference approximation.[46] According to Parr and Yang,[46] the higher FF values point to the more reactivity of the atom than others.

Molar refractivity (MR) is an important property used in quantitative structure property relationship. It is calculated by the Lorentz–Lorentz equation[47,48] and is defined as:

$$MR = \left[\frac{n^2-1}{n^2+2}\right]\left(\frac{MW}{\rho}\right) = 1.333\,\pi N\alpha,$$

while n is the refractive index; MW is the molecular weight; ρ is the density; (MW/ρ) is the molar volume; N is the Avogadro number; α is the polarizability of the molecular system.

In NBO analysis, the hyper conjugative interaction energy was deduced from the second-order perturbation approach[49]

$$E^{(2)} = -q_i\left[\frac{(F_{ij})^2}{\epsilon_i - \epsilon_j}\right]$$

where, q_i is the population of donor orbital or donor orbital occupancy; ε_i, ε_j are orbital energies of donor and acceptor NBO orbitals, respectively; F_{ij} is the off-diagonal Fock or Kohn-Sham matrix element between i and j NBO orbitals.

Espinosa[50] proposed proportionality between hydrogen bond energy (E) and potential energy density (V_{BCP}) at H···O contact:

$$E_{HB} = \frac{1}{2}V_{BCP}$$

V. Results and discussion

1. Geometry optimization and energies

NF-3ABA (1:1) cocrystal crystallizes in the triclinic system in the space group P$\bar{1}$ with one molecule each of NF and 3ABA adopting planar conformation in the asymmetric unit.[51] As far as the crystallographic structure of NF-3ABA is concerned, the imide of NF and acid of 3ABA form an O–H···O and N–H···O interactions as shown in the Fig 1. It was noted there is a C–H···O dimer is formed between the activated C–H and nitro group of furyl ring in NF. Next, the primary NH_2 of 3ABA is involved in bifurcated N–H···O and N–H···N interactions with the available O/N acceptors of NF. The solid-state packing is further supported by C–H···O interactions to complete a sheet structure.[51] In present calculation, the planer configuration of NF-3ABA (1:1) has been adopted for calculating the different properties. Initial geometry optimization of NF-3ABA (1:1) was performed using the crystallographic data of cocrystal reported by one of the authors of current work.[51] Initial geometry for NF (API), 3-ABA (co-former), and NF-3ABA (cocrystal) was minimized at the DFT level employing B3LYP/cc-pvTZ and wB97X-D/cc-pvTZ level of theory.

The ground state optimized structure of NF-3ABA, NF, and 3ABA using wB97X-D/cc-pvTZ are shown in Fig. 1 and in electronic supplementary information (ESI†, see Fig. S1 and Fig. S2). The optimized structural parameters (bond lengths, bond angles, and dihedral angles) of the NF and NF-3ABA cocrystal were also compared with the experimental results (See also Table S1, ESI†).[51]

View Article Online
DOI: 10.1039/C7CE00864C

It may be seen that both the functional yield comparable geometries, which differ from the experimental geometry[51] by not more than 0.02 Å in bond length except for the bonds having one of the atoms as hydrogen. A comparison of the bond angles shows that calculations can replicate the experimental data within 3.1° in bond angles and 5.4° in dihedral angles. The calculated bond length of N–H and C=O bonds of the hydantoin ring in pure NF was found to be 1.0076 Å and 1.2023 Å, respectively, whereas in NF-3ABA it was found to be 1.0297 and 1.2185 Å, respectively. The variations in the bond length of N-H and C=O bonds NF-3ABA are due to the presence of H-bonds between NF and 3ABA, which has resulted in the increment of bond lengths.

The ground state energy of the NF-3ABA was calculated using B3LYP/cc-pvTZ and wB97X-D/cc-pvTZ are −1380.17103 a.u. and −1379.70158 a.u., respectively. In the NF-3ABA, intermolecular hydrogen bonds were formed between NF and 3ABA. E_{int} can be computed using either supermolecular or perturbative approach. In this work, DFT methods (such as B3LYP, and ωB97X-D) are used to obtain E_{int} within the framework of the supermolecular approach. According to former, the interaction energy of the analyzed NF-3ABA was computed as the difference between the calculated total energy of the NF-3ABA and the energies of the two isolated molecules i.e. NF and 3ABA. The total energy of NF and 3ABA was calculated using wB97X-D/cc-pvTZ (B3LYP/cc-pvTZ) is –903.48793 (−903.78559) a.u. and –476.19615 (−476.36336) a.u. respectively. Therefore, the interaction energy (E_{int}) of the NF-3ABA were calculated using wB97X-D/cc-pvTZ and B3LYP/cc-pvTZ as −17.85 kcal/mol and −15.76 kcal/mol, respectively. The interaction energies may be influenced by the basis set superposition error (BSSE), which is generally amended by the counterpoise (CP) method of Boys and Bernardi.[52] The calculated E_{int} of NF-3ABA has been corrected for the basis set superposition error (BSSE) via the standard counterpoise method[52] and found to be −16.76 kcal/mol and −14.51 kcal/mol using wB97X-D/cc-pvTZ and B3LYP/cc-pvTZ, respectively.

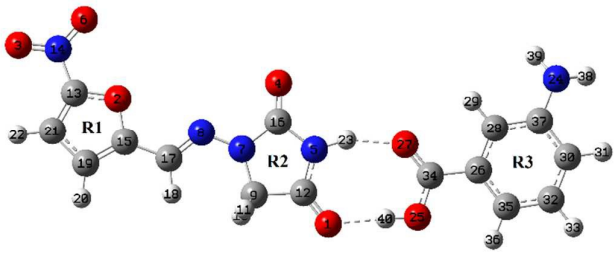

Fig. 1 Optimized structure for NF-3ABA using wB97X-D/cc-pvTZ method and the atom numbering scheme adopted in this study.

2. Vibrational spectra

Total number of atoms in NF-3ABA, NF and 3-ABA are 40, 23 and 17 and it gives 114, 63 and 45 (3N−6) (N-number of atoms) normal modes of vibrations respectively, all active in infrared and Raman spectra. The recorded and calculated vibrational wavenumbers at the wB97X-D/cc-pvTZ and B3LYP/cc-pvTZ for NF-3ABA and their probable assignments with PED are given in Table S2 and Table S3 (ESI†) respectively. The theoretical and experimental vibrational wavenumbers of NF (API) and 3ABA (co-former) calculated at wB97X-D/cc-pvTZ and B3LYP/cc-pvTZ methods and their assignments using PED are given in Table S4 and S5 (ESI†) respectively. Here the mode with maximum contribution is accepted to be the most significant mode.

This is obvious that the frequencies calculated based on quantum mechanical force fields usually differ appreciably from observed frequencies. This difference between calculated and observed spectra can be attributed to several factors. Firstly, to the environment (gas and solid phase) and secondly due to neglect of anharmonicity effects present in a real system. Frequency calculations were performed in the limit of the harmonic approximation. Therefore, calculated wavenumbers are scaled down using the scaling factor 0.965[53] for B3LYP/cc-pvTZ and 0.956[54] for wB97X-D/cc-pvTZ to discard anharmonicity present in the real system. The comparison among calculated and observed FT-IR and FT-Raman spectra of NF-3ABA is shown graphically in Figs. 2 and 3, respectively. Comparison of experimental and calculated (scaled) IR and Raman spectra of NF and 3ABA are shown in Figs. S3–S6 (ESI†).

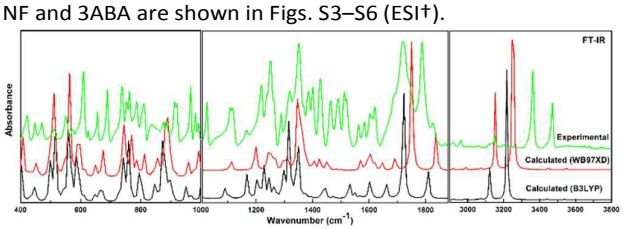

Fig. 2 Experimental and calculated (WB97XD and B3LYP) IR spectra of NF-3ABA.

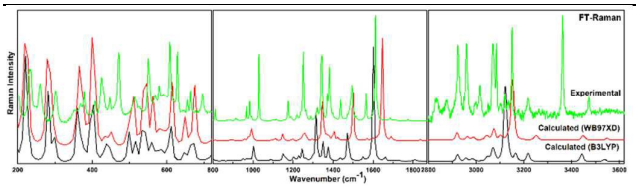

Fig. 3 Experimental and calculated (WB97XD and B3LYP) Raman spectra of NF-3ABA.

3. ^{13}C NMR chemical shift

In the present work, NMR chemical shifts for NF-3ABA, NF (API) and 3ABA (co-former) were computed with the B3LYP[30] and wB97X-D[33] functionals and the cc-pVTZ basis set[29] using GIAO method. The rationalisation behind the selection of these functional was to include the most frequently used hybrid functional (B3LYP) and one long range-corrected hybrid including dispersion corrections (wB97X-D). To compare the predicted values with experimental results, we also need to compute the absolute shielding value for the TMS, using the same model (level of theory, basis set and method of geometry optimization). To further examine the intermolecular interactions between nitrofurantoin and 3-aminobenzoic acid, the ^{13}C CP-MAS solid state NMR spectra of the NF-3ABA, NF and 3ABA were determined are shown in Fig. 4. The experimental and calculated ^{13}C NMR chemical shifts of NF-3ABA, NF and 3ABA are recorded in Table S6 (ESI†). The highest ^{13}C chemical shifts of C12 and C34 at 174.602 ppm and 171.077 ppm, which shows the bonding with the electron attracting species (here O and N) as shown in Fig 1 in the case of NF-3ABA cocrystal. A single peak is observed for the carbon atoms having same surroundings. The rest of the carbon atoms peaks of NF-3ABA are in the range of 47.950-150.811 ppm. The comparison between the spectra of NF and the NF-3ABA showed that the peak at position 168.9 ppm,

View Article Online
DOI: 10.1039/C7CE00864C
CrystEngComm PAPER

which was allotted to C11=O in NF, shifted to 174.602 ppm in the NF-3ABA. Thus, the environment of C11=O in NF had changed after cocrystal formation. This shift could be attributed to the change in the environment of the neighbouring –OH. Table S6 (ESI†) shows that calculated chemical shifts, which matches well with that of experimental values. The mean absolute errors for the same basis set with different functionals were calculated to identify the effect of different functional. The mean absolute errors for different functional are given in Table S7 (ESI†). Mean absolute error when considering same basis set with different functionals B3LYP and wB97X-D were 4.46 ppm and 3.87 ppm respectively for NF-3ABA and 3.29 ppm and 2.60 ppm respectively for NF. We found that wB97X-D functional was the best for calculating ^{13}C chemical shifts (with GIAO approaches) in comparison to B3LYP functional.

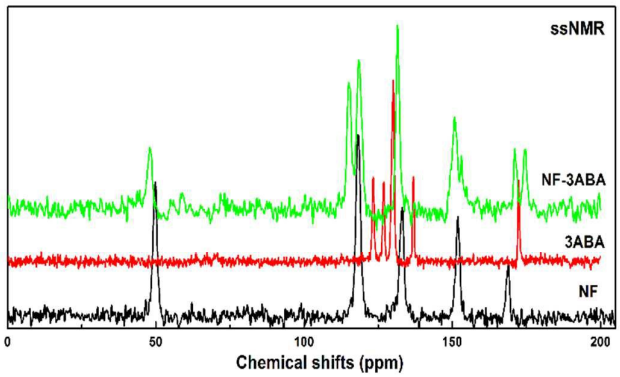

Fig. 4 Experimental ^{13}C NMR spectrum of NF, 3ABA and NF-3ABA cocrystal.

Least square regressions were employed to determine the quality of the linear relationship; y = mx + C, where x is the calculated ^{13}C NMR chemical shifts (δ in ppm), m is the slope, y is the experimental ^{13}C NMR chemical shifts (δ in ppm) and C is the constant, between the experimental and the calculated chemical shifts. The linear relationship as well as the fit equation for data obtained with the GIAO/wB97X-D/cc-pVTZ method for NF-3ABA and NF is shown in Fig. S8 (ESI†). As illustrated in Fig. S8, the coefficients of determination values (R^2) for NF-3ABA and NF ^{13}C NMR are equal to 0.9975 and 0.9964, respectively. This shows that there is a good agreement between experimental and calculated ^{13}C NMR chemical shifts.

4. Natural bond orbital analysis (NBO)

NBO analysis is one of the efficient methods for studying the role of intermolecular and intramolecular orbital interaction and knowing about charge transfer and conjugative interactions in the complex. NBO offers quick understanding of the bonding in the molecules. NBO analysis is performed by considering all possible interactions between filled donor Lewis-type and empty acceptor Lewis-type NBOs and predicting their energetic significance by second-order perturbation theory. In the present work, taking the advantage of the second-order perturbation theory analysis, herein we report some of the electron donor and acceptor orbitals and the interaction stabilization energy. The intensity of the interaction between electron donors and electron acceptors, i.e. the propensity of donating more electrons from donors to acceptors depend on the $E^{(2)}$ value. NBO analysis has been performed on the title compound at the wB97X-D/cc-pvTZ and B3LYP/cc-pvTZ level to explain the intra-molecular rehybridization and delocalization of electron density within the molecule. Table S8 and S9 (ESI†) summarizes the selected second-order perturbative estimates of ''donor–acceptor'' (bond–antibond) interactions in the NBO basis for the NF-3ABA, which shows π-conjugation/resonance due to π-electron delocalization in ring, primary and secondary hyper conjugative interactions. The calculated stabilization energy using B3LYP/cc-pvTZ are given in parenthesis. Here only those hyperconjugative interactions are discussed which are involve in the hydrogen bonding and show high stabilization energy.

The primary hyperconjugative interactions n_2(O1) → σ*(N5–C12)/σ*(C9–C12), n_2(O2) → π*(C13–C21)/π*(C15–C19), n_2(O3) → σ*(O6–N14)/σ*(C13–N14), n_3(O3) → π*(O6–N14), n_2(O4) → σ*(N5–C16)/σ*(N7–C16), n_2(O6) → σ*(O3–N14)/σ*(C13–N14), n_1(O25) → σ*(O27–C24), n_2(O25) → π*(O27–C34), and n_2(O27) → σ*(O25–C34)/σ*(C26–C34) are stabilized the molecule to a greater extent ~157.41 kcal/mol. The other interactions n_1(N5) → π*(O1–C12)/π*(O4–C16), n_1(N7) → π*(O4–C16)/π*(N8–C17), n_1(N8) → σ*(N7–C9)/σ*(C17–H18) and n_1(N24) → π*(C28–C37) are also stabilized the molecule with maximum energy ~239.34 (~73.47) kcal/mol.

The primary hyperconjugative interaction from unit (1) to unit (2) due to n_1(O1)/n_2(O1) → σ*(O25–H40) stabilized the molecule up to ~17.88 (~14.19) kcal/mol and confirms the presence of interaction O25–H40···O1. Another intermolecular interaction from unit (2) to unit (1) due to n_1(O27)/n_2(O27) → σ*(N5–H23) stabilized the molecule up to ~12.04 (~9.58) kcal/mol and confirms the presence of interaction N5–H23···O27.

5. QTAIM calculation: Topological parameters at bond critical points (BCP)

The quantum theory of atoms in molecules (QTAIM) theory provides a significant amount of information about the properties of any chemical bonds including hydrogen bonds. The theory of QTAIM well describes H-bonding and its concept. Bond critical point (BCP) is used in the identification of chemical bonds between atoms and interatomic interaction. The QTAIM method gives information about the ED region of a system and governs properties at BCPs. Geometrical and topological parameters are useful tools to characterise the strength and nature of the H-bond. Koch and Popelier[55] proposed a set of criteria for the existence of H-bond based on AIM theory. The criteria provide a basis to distinguish these interactions from van der Waals interactions and have been proved to be valid for standard and non-conventional H-bonds. According to Rozas et al.,[56] the interactions may be classified as follows: (i) for strong H-bonds ($\nabla^2\rho_{BCP}) < 0$, $H_{BCP} < 0$and covalent in nature, (ii) for medium H-bonds ($\nabla^2\rho_{BCP}) > 0$, $H_{BCP} < 0$ and partially covalent in nature and (iii) for weak H-bonds ($\nabla^2\rho_{BCP}) > 0$ and $H_{BCP} > 0$ and electrostatic in nature.

Molecular graph of the NF-3ABA using AIM program at wB97X-D/cc-pvTZ level is given in Fig. 5. Geometrical as well as topological parameters for bonds of interacting atoms in NF-3ABA are given in Table 1. Based on these parameters, O1···H40 and O27···H23 are moderate hydrogen bonds. The nature of these H-bonds is partially covalent due to ($\nabla^2\rho_{BCP}) > 0$ and $H_{BCP} < 0$. The various types of interactions visualized in molecular graph are classified based on geometrical, topological and energetic parameters. In this article,

View Article Online
DOI: 10.1039/C7CE00864C

the Bader's theory application has been used to estimate hydrogen bond energy (E). The energy of these H-bonds is calculated as −11.60/−12.34 and −10.22/−10.79 kcal/mol using B3LYP/wB97X-D funtionals, respectively and their strengths are in the following order: O1···H40 > O27···H23. The results obtained by QTAIM theory is also validated with the help of the reduced density gradient (RDG) and the isosurface analysis using Multiwfn software[57] (ESI†).

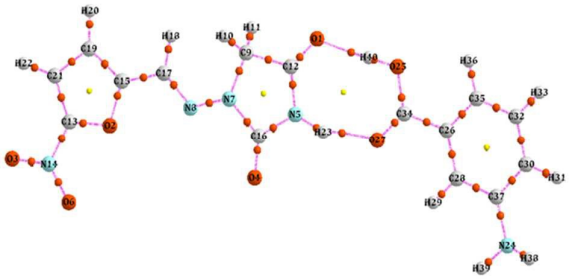

Fig. 5 Molecular graph of the NF-3ABA using AIM program at wB97X-D/cc-pvTZ method: bond critical points (small red spheres), ring critical points (small yellow sphere), and bond paths (pink lines).

Table 1 Geometrical parameters (bond length) and topological parameters for bonds of interacting atoms: electron density (ρ_{BCP}), Laplacian of electron density ($\nabla^2\rho_{BCP}$), electron kinetic energy density (G_{BCP}), electron potential energy density (V_{BCP}), total electron energy density (H_{BCP}) at bond critical point (BCP) and estimated hydrogen bond energy (E_{intHB}).

Interactions	Bond length (Å)	ρ_{BCP} (a.u.)	$\nabla^2\rho_{BCP}$ (a.u.)	G_{BCP} (a.u.)	V_{BCP} (a.u.)	H_{BCP} (a.u.)	E_{HB} (kcal/mol)
Using wB97X-D/cc-pvTZ							
C12-O1···H40	1.73927	0.0415	0.0945	0.0078	-0.0393	-0.0315	-12.3437
N5-H23···O27	1.77664	0.0379	0.1055	0.0040	-0.0344	-0.0304	-10.7894
Using B3LYP/cc-pvTZ							
C12-O1···H40	1.75671	0.035297	0.116141	0.02936	-0.0297	-0.00032	-9.3123
N5-H23···O27	1.79170	0.03264	0.114381	0.027718	-0.0268	0.000878	-8.4212

6. Frontier Molecular Orbitals (FMOs) analysis

The frontier molecular orbital plays a significant role in the electric and optical properties of the molecule.[58,59] Highest occupied molecular orbital (HOMO) and lowest unoccupied molecular orbital (LUMO) energies are very important parameters for quantum chemical calculations. HOMO energy characterizes the capability of electron giving and LUMO energy is related to the electron affinity. To calculate the reactivity of the molecule, the energies of HOMO, LUMO and HOMO–LUMO energy gaps are calculated using wB97X-D/cc-pvTZ and B3LYP/cc-pvTZ basis sets for the both NF and NF-3ABA.

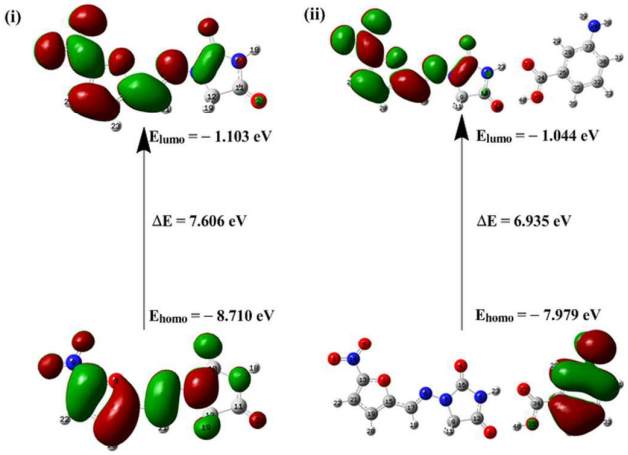

Fig. 6 HOMO-LUMO plot of NF-3ABA cocrystal with orbitals involved in electronic transitions in isolated (gaseous) phase (i) using wB97X-D/cc-pvTZ method (ii) using B3LYP/cc-pvTZ method.

The features of the HOMO and LUMO for NF and NF-3ABA with energy values can be seen in Figs. S11 (ESI†) and 6. The HOMO-LUMO energy gap reflects the chemical reactivity of NF and NF-3ABA. A small gap implies high chemical reactivity (low stable) and large gap implies less chemical reactivity (highly stable).[60] The stability of molecule can also be related to hardness; the lower stability indicates that the molecule is more softer and hence more reactive. This can be confirmed by global reactivity descriptors as well. The calculated HOMO–LUMO gap for NF and NF-3ABA using wB97X-D/cc-pvTZ is −7.606 and −6.935 eV respectively, whereas calculated HOMO–LUMO gap for NF and NF-3ABA using B3LYP/cc-pvTZ is −3.7843 and −3.0558 eV respectively. The energy gap reflects same pattern by both the functionals as shown in Figs. S11 and 6. After the formation of NF-3ABA, the energy gap decreases, this represents higher electronic transitions. So, chemical reactivity of NF-3ABA is higher than NF.

7. Chemical reactivity descriptors

Global reactivity descriptor helps in prediction of electrophilic and nucleophilic reagent, whereas local reactivity descriptors help in the prediction of the site of electrophilic and nucleophilic attack as well as the order of preference.

7.1. Global reactivity descriptors

Electronegativity (χ), chemical potential (μ), global hardness (η), global softness (S) and electrophilicity index (ω) these all are global reactivity descriptors, exceptionally effective in predicting global reactivity trends.

The energies of frontier molecular orbitals (E_{HOMO}, E_{LUMO}), energy band gap ($E_{HOMO} - E_{LUMO}$), χ, μ, η, S and ω for NF, 3ABA, NF-3ABA are listed in Table 2. The chemical hardness (η) and softness (S) of a molecule is a good indication of the chemical stability of the molecule. The molecules with a large energy gap are known as hard molecule whereas molecules having a small energy gap are known as soft molecules. The soft molecules are more polarizable than the hard ones. The η is a direct measure of the electrophilic stability of a molecule, while S provides a measure of its electrophilic reactivity. The computed η for NF, 3ABA, NF-3ABA is in the order of 3ABA > NF > NF-3ABA, and the value of S is in the order of NF-3ABA > NF > 3ABA. Therefore, the ability of soaking up of electrons

View Article Online
DOI: 10.1039/C7CE00864C
CrystEngComm PAPER

for NF is more prominent and tendency to contribute the electrons is more in the case of NF-3ABA. The ω as another useful reactivity descriptor also quantifies the tendency of a molecule to soak up electrons. A molecule with the high value of ω shows the great propensity of attracting electrons from a generic donor molecule. The calculated ω found in the order: NF-3ABA > NF > 3ABA indicating that NF-3ABA has an obvious capacity to accept electrons (strong electrophile) than NF (API) and 3ABA (coformer).

Electrophilic charge transfer (ECT) is calculated as 0.4106 and 0.9866 using wB97X-D and B3LYP fuctionals respectively for reactant molecules NF and 3ABA, which indicates that charge flows from 3ABA to NF as ECT > 0. Therefore, NF acts as electron acceptor and 3ABA as electron donor. The low value of chemical potential and high value of electrophilicity index for NF favor its electrophilic behavior. In the same way, the high value of chemical potential and low value of electrophilicity index for 3ABA favour its nucleophilic behavior.

Table 2 Calculated E_{HOMO}, E_{LUMO}, energy band gap (E_H-E_L), chemical potential (μ), electronegativity (χ), global hardness (η), global softness (S) and global electrophilicity index (ω) at 298.15 K for NF, 3ABA and NF-3ABA.

Molecule	E_H (eV)	E_L (eV)	E_H-E_L (eV)	χ (eV)	μ (eV)	η (eV)	S (eV^{-1})	ω (eV)	ΔN_{max}	ECT
Using B3LYP/cc-pvTZ										
NF	-6.854	-3.070	3.784	4.962	-4.962	1.892	0.264	6.5066	2.6225	
3ABA	-6.012	-1.450	4.561	3.731	-3.731	2.281	0.219	3.0519	1.6359	0.9866
NF-3ABA	-6.063	-3.007	3.056	4.535	-4.535	1.528	0.327	6.7311	2.9683	
Using WB97XD/cc-pvTZ										
NF	-8.71	-1.103	7.606	4.9066	-4.907	3.803	0.131	3.165	1.29	
3 ABA	-7.94	0.509	8.449	3.7153	-3.715	4.224	0.118	1.634	0.879	0.4106
NF-3ABA	-7.979	-1.044	6.935	4.5115	-4.511	3.468	0.144	2.935	1.301	

7.2. Local reactivity descriptors

Using Hirshfeld atomic charges of neutral, cation and anion state of NF-3ABA, Fukui Function (FF) (f_k^+, f_k^-, f_k^0), local softnesses (s_k^+, sk^-, sk^0) and local electrophilicity indices (ω_k^+, ω_k^-, ω_k^0) were calculated. Fukui functions, local softnesses and local electrophilicity indices for selected atomic sites in NF-3ABA have been listed in Table S10 (ESI†). The calculated local electronic descriptors (f_k^+, s_k^+, ω_k^+), (f_k^-, s_k^-, ω_k^-), (f_k^+/f_k^-) and (f_k^- /f_k^+), (f_k^+/f_k^-) and (f_k^- /f_k^+) ratio values are only capable for providing a clear distinction between more reactive atomic centres. The maximum values of all the three local electrophilic reactivity descriptors (f_k^+, s_k^+, ω_k^+) and the highest ratio value of (f_k^+/f_k^-) at N7 indicate that this site has greater chance of attacking the nucleophilic site of the other molecules. The maximum values of all the three local nucleophilic reactivity descriptors (f_k^-, s_k^-, ω_k^-) for O3, O6 and N14 atoms found to be (0.1322, 0.01906, 0.38797), (0.1272, 0.01834, 0.3733) and (0.07236, 0.01043, 0.21235) respectively. The highest ratio value of (f_k^- /f_k^+) at N14 of nitro group indicates that this site is more reactive then O3 and O6 oxygen. Therefore, the nitrogen atom (N14) has greater possibility of attacking the electrophilic site of the other molecules.

The pictorial representation of these electrophilic and nucleophilic atomic sites of NF-3ABA is shown by molecular electrostatic potential surface analysis (ESI†).

8. Molar refractivity (MR)

The MR reflects the dispersivity of the valence electrons, which depends on the mass, charge, and polarizability of the molecule. MR is also related to volume of the molecule and London dispersive force, which act in the ligand-receptors interactions. This is an important property for estimating the biological activity of NF-3ABA. For (MR), the succeeding range is between 40 e.s.u. and 130 e.s.u., with an average value of 97.[61] The value of the MR for NF-3ABA is 55.78 and 55.10 e.s.u using wB97X-D/cc-pvTZ and B3LYP/cc-pvTZ level of theory respectively. Here this value of MR is responsible for the polarizability and reactivity of the NF-3ABA which is an important feature concerning pharmaceutical point of view.

VI. Conclusions

An effective study has been performed on the structural and spectral characteristics of an API, NF, and NF-3ABA cocrystal by experimental spectroscopic methods and quantum chemical calculations. The performance of different methods (experimental and theoretical) has been investigated to elucidate the variation of properties of nitrofurantoin-3-aminobenzoic acid cocrystal and to study the hydrogen bond interactions. Spectral analysis shows that imide N-H, C=O group of hydantoin ring in NF interact with acid C=O, -OH in 3ABA to form NF-3ABA cocrystal. Red shift in the stretching wavenumber is observed in the case NF-3ABA in comparison to NF due to hydrogen bonding functionalities such as NH, OH and C=O causes elongation in the corresponding bond lengths in NF-3ABA. The solid-state NMR spectra provided further evidence of the intermolecular interactions in the NF-3ABA cocrystal. The theoretically constructed IR and Raman spectra of NF-3ABA using wB97X-D/cc-pvTZ level of theory shows good correlation with experimentally observed ones. For calculating ^{13}C NMR shifts, the best results for ^{13}C was obtained with wB97X-D/cc-pVTZ method with GIAO approaches (mae =3.29 ppm and 2.60 ppm for NF-3ABA and NF respectively). Therefore, the results suggest that wB97X-D is best applied DFT functional to describe the hydrogen bonding interactions in comparison to B3LYP. Topological, geometrical and energetic parameters calculated using QTAIM suggest that the O1···H40 and O27···H23 are moderate in nature as ($\nabla^2\rho_{BCP}$) > 0, H_{BCP} < 0 with the maximum interaction energy E_{int} = 12.34 kcal/mol. The calculated interaction energy (E_{int}) of NF-3ABA using wB97X-D/cc-pvTZ and B3LYP/cc-pvTZ DFT methods are −16.76 and −14.51 kcal/mol respectively. The HOMO-LUMO energy band gap explain the activity of the molecule, concluding that NF-3ABA is more reactive than NF. Global electrophilicity index (ω = 6.7311 eV) shows that NF-3ABA is a stronger electrophile than NF and 3ABA. From the molecular electrostatic potential (MEP) map and reactivity descriptor calculations, the NO_2 group is suitable for electrophilic attack

View Article Online
DOI: 10.1039/C7CE00864C

in NF-3ABA. The calculated value of electrophilic charge transfer ECT > 0 indicating that the charge flows from 3ABA to NF during NF-3ABA formation. Thus, NF behaves as electron acceptor and 3ABA as electron donor. Molar refractivity value (55.78 e.s.u.) of NF-3ABA lies in the range set for drug likeness. As a result, cocrystal may be used as an orally active drug. The calculations which we performed in this manuscript have wide scope in the drug discovery. Moreover, reactivity is a primary step for the identification of chemical properties of the drug molecule. Hence, we hope that the studies performed on NF-3ABA cocrystal will be of significant impact in the spectroscopy field as well as pharmaceutical industry.

Acknowledgements

Solid-state NMR spectra for NF, 3ABA and NF-3ABA were obtained at the EPSRC UK National Solid-state NMR Service at Durham. We are thankful to Prof. Alejandro P Ayala, Departamento de Física, Universidade Federal do Ceará, Fortaleza, Brasil for performing FT-Raman of the cocrystal. We thank Mr Niten Jadhav and Dr Richard Telford for their helpful discussions. A. Shukla thanks financial assistance from the DST (New Delhi) under the DST purse programme. E. Khan and K. Srivastava are thankful for the support from the UGC under BSR meritorious fellowship scheme. P. Tandon acknowledges the financial support provided by the DST, India under the Indo-Brazil project. V. R. Vangala acknowledges the financial support of the Royal Society of Chemistry for mobility grant (2015/17).

References

1 N. K. Duggirala, M. L. Perry, Ö. Almarsson and M. J. Zaworotko, *Chem. Commun.*, 2016, **52**, 640–655.
2 S. Aitipamula, R. Banerjee, A. K. Bansal, K. Biradha, M. L. Cheney, A. R. Choudhury, G. R. Desiraju, A. G. Dikundwar, R. Dubey, N. Duggirala, P. P. Ghogale, S. Ghosh, P. K. Goswami, N. R. Goud, R. R. K. R. Jetti, P. Karpinski, P. Kaushik, D. Kumar, V. Kumar, B. Moulton, A. Mukherjee, G. Mukherjee, A. S. Myerson, V. Puri, A. Ramanan, T. Rajamannar, C. M. Reddy, N. Rodriguez-Hornedo, R. D. Rogers, T. N. G. Row, P. Sanphui, N. Shan, G. Shete, A. Singh, C. C. Sun, J. A. Swift, R. Thaimattam, T. S. Thakur, R. Kumar Thaper, S. P. Thomas, S. Tothadi, V. R. Vangala, N. Variankaval, P. Vishweshwar, D. R. Weyna and M. J. Zaworotko, *Cryst. Growth Des.* 2012, **12**, 2147-2152.
3 E. R. T. Tiekink, J. J. Vittal, *Wiley Online Library*, 2006, 25-49.
4 (a) C. B. Aakeröy, D. J. Salmon, *CrystEngComm* 2005, **7**, 439–448; (b) N. J. Babu, A. Nangia, *Cryst. Growth Des*., 2011, **11**, 2662–2679.
5 (a) A. V. Trask, *Mol. Pharm*., 2007, 4, 301-309; (b) N. Rodríguez-Hornedo, *Mol. Pharmaceutics,* 2007, **4**, 299–300; (c) O Almarsson, M. J. Zaworotko, *Chem. Commun (Camb)*, 2004,**17**, 1889–1896.
6 (a) S. L. Childs, L. J. Chyall, J. T. Dunlap, V. N. Smolenskaya, B. C. Stahly, G. P. Stahly, *J. Am. Chem. Soc.,* 2004, **126**, 13335–13342; (b) N. Variankaval, R. Wenslow, J. Murry, R. Hartman, R. Helmy, E. Kwong, S. D. Clas, C. Dalton, I. Santos, *Cryst. Growth Des.*, 2006,**6**, 690–700; (c) V. R. Vangala, P. S. Chow, R. B. H. Tan, *CrystEngComm*, 2011, **13**, 759-762; (d) MHD.B. Alsirawan, V. R. Vangala, J. Kendrick, F. J. J. Leusen, A. Paradkar, *Cryst. Growth Des.* 2016, **16**, 3072-3075. (e) S. Aitipamula, V. R. Vangala, P. S. Chow, R. B. H. Tan, *Cryst. Growth Des*., 2012, **12**, 5858-5863; (f) C. C. Sun, H. Hou, *Cryst. Growth Des.* 2008, **8**, 1575-1579.
7 R. Eyjolfsson, *Drug Dev. Ind. Pharm.* 1999, **25**, 105-106.
8 E. W. Pienaar, M. R. Caira, A. P. Lotter, *J. Cryst. Spectrosc. Res.,* 1993, **23**, 785-790.
9 V. Bertolasi, P. Gilli, V. Ferretti, G. Gilli, *Acta Cryst.,* 1993, **C49**,741-744.
10 P. V. Marshall, P. York, *Int. J. Pharm.* 1989, **55**, 257-263.
11 (a) H. W. Gouda, M. A. Moustafa, H. I. Al-Shora, *Int. J. Pharm*., 1984, **18**, 213–215; (b) A. E. A. R. Ebian, R. M. A. Moustafa, E. B. Abul-Enin, Egypt. *J. Pharm. Sci.*, 1985, **26**, 287–300; (c) A. E. A. R. Ebian, H. T. Fikrat, R. M. A. Moustafa, E. B. Abul-Enin, Egypt. *J. Pharm. Sci*., 1986, **27**, 347–358.
12 M. Otsuka, R. Teraoka, Y. Matsuda, *Pharm. Res.*, 1991, **8**, 1066.
13 S. Karki, T. Friščić, L. Fábián, P. R. Laity, G. M. Day, W. Jones, *Adv. Mater*., 2009, **21**, 3905–3909.
14 N. Blagden, M. de Matas, P. T. Gavan, P. York, *Adv. Drug Delivery Rev*., 2007, **59**, 617–630.
15 (a) G. Bolla, A. Nangia, *Chem. Commun.* 2016, **52**, 8342-8360; (b) D. P. Kale, S. S. Zode, A. K. Bansal, *J. Pharm. Sci.* 2017, **106**, 457-470.
16 (a) D. P. McNamara, S. L. Childs, J. Giordano, A. Iarriccio, J. Cassidy, M. S. Shet, R. Mannion, E. O'Donnel, A. Park, *Pharm. Res.,* 2006, **23**, 1888–1897; (b) M. B. Hickey, M. L. Peterson, L. A. Scoppettuolo, S. L. Morrisette, A. Vetter, H. Guzm_an, J. F. Remenar, Z. Zhang, M. D. Tawa, S. Haley,M. J. Zaworotko, Ö. Almarsson, Eur. *J. Pharm. Biopharm*., 2007, **67**, 112–119.
17 H. C. Stephen Chan, J. Kendrick, M. A. Neumann, F. J. J. Leusen, *CrystEngComm*, 2013, **15**, 3799.
18 M. Sacchi, A. Y. Brewer, S. J. Jenkins, J. E. Parker, T. Friščić, S. M. Clarke, *Langmuir* 2013, **29**, 14903–14911.
19 K. Srivastava, M. R. Shimpi, A. Srivastava, P. Tandon, K. Sinha, S. P. Velaga, *RSC Adv.*, 2016, **6**, 10024-10037.
20 J. Pandey, P. Prajapati, M. R. Shimpi, P. Tandon, S. P. Velaga, A. Srivastava, K. Sinha, *RSC Adv*., 2016, **6**, 74135-74154.
21 H. Eshtiagh-Hosseini, H. Aghabozorg, M. Mirzaei, S. A. Beyramabadi, H. Eshghi, A. Morsali, A. Shokrollahi, R. Aghaei, *Spectrochimica Acta Part A: Molecular and Biomolecular Spectroscopy*, 2011, **78**, 1392–1396.
22 X. Li, M. A. Neumann, J. van de Streek, *IUCrJ*, 2017, **4**, 175-184.
23 Goar Sa´nchez-Sanz, Cristina Trujillo, Ibon Alkorta and Jose´ Elguero, *Phys.Chem.Chem.Phys.,* 2016, 18, 9148.
24 Piotr Matczak, *J Mol Model*, 2016, 22, 208.
25 C. F. Matta, R. J. Boyd, *Wiley-VCH*, Weinheim, 2007, 567.
26 P. Hohenberg, W. Kohn, Phys. Rev., 1964, **136B**, 864–871.
27 M. J. Frisch, G. W. Trucks, H. B. Schlegel, G. E. Scuseria, J. R. Cheeseman, M. A. Robb, G. Scalmani, V. Barone, B. Mennucci, G. A. Petersson, H. Nakatsuji, M. Caricato, X. Li, H. P. Hratchian, A. F. Izmzylov, J. Bloino, G. Zheng, J. L. Sonnenberg, M. Hada,M. Ehara, K. Toyota, R. Fukuda, J. Ishida, M. Hasegawa, T. Nakajima, Y. Honda, O. Kitao, H. Nakai, T. Vreven, J. A. Montgomery, J. E. Peralta Jr., F. Ogliaro,M. Bearpark, J. J. Heyd, E. Brothers, K. N. Kudin, V. N. Staroverov, R. Kobayashi, J. Normand, A. Raghavachari, A. Rendell, J. C. Burant, S. S. Iyengar, J. Tomasi, M. Cossi, N. Rega, J. M. Millan, M. Klene, J. E. Knox, J. B. Cross, V. Bakken, C. Adamo, J. Jaramillo, R. Gomperts, R. E. Stratmann, O. Yazyev, A. J. Austin, R. Cammi, C. Pomelli, J. W. Ochterski, R. L. Martin, K. Morokuma, V. G. Zakrzewski, G. A. Voth, P. Salvador, J. J. Dannerberg, S. Dapprich, A. D. Daniels, J. Farkas, B. Foresman, J. V. Ortiz, J. Cioslowski and D. J. Fox, GAUSSIAN 09, Revision, Gaussian, Inc., Wallingford CT, 2009.
28 T. H. Dunning, Jr., *J. Chem. Phys.*, **1989**, *90*, 1007-1023.
29 D. E. Woon, T. H. Dunning, Jr., *J. Chem. Phys.*, 1995, ***103***, 4572-4585.
30 A. D. Becke, *J Chem Phys.*,1993, **98**, 5648–5652.

View Article Online
DOI: 10.1039/C7CE00864C

31 C. T. Lee, W. T. Yang, R. G. Parr, *Phys. Rev*. 1988, **37B**, 785-789.
32 R. G. Parr and W. Yang, Density Functional Theory of Atoms and Molecules, Oxford, New York, 1989.
33 J.-D. Chai, M. Head-Gordon, *Phys. Chem. Chem. Phys.*, 2008, **10**, 6615-6620.
34 K. Wilson, T. van Mourik, and T. H. Dunning, Jr., *J. Mol. Struct.: THEOCHEM***,** 1996, **338**, 339-349.
35 D. E. Woon, K. A. Peterson, T. H. Dunning, Jr., *J. Chem. Phys*., 1998, **109**, 2233-2241.
36 A. K. Wilson, D. E. Woon, K. A. Peterson, T. H. Dunning, Jr., *J. Chem. Phys*., 1999 **110**, 7667-7676.
37 P. Pulay, G. Fogarasi, F. Pang, J. E. Boggs*, J. Am. Chem. Soc.*, 1979, **101,** 2550–2560.
38 J.M.L. Martin, C. Van Alsenoy, Gar2ped, University of Antwerp, 1995.
39 A. Frisch, A. B. Nielson, A. J. Holder, GaussView User Manual, Gaussian Inc, Pittsburgh, PA, 2005.
40 R. F. W. Bader, J. R. Cheeseman, AIMPAC, 2000.
41 G. A. Guirgis, P. Klaboe, S. Shen, D. L. Powell, A. Gruodis, V. Aleksa, C. J. Nielsen, J. Tao, C. Zheng, J. R. Durig, *J. Raman Spectrosc*., 2003, **34**, 322–336.
42 K. Wolinski, J.F. Hinton, J.F. Pulay, *J. Am. Chem. Soc*., 1990, **112,** 8251-8260.
43 R. G. Parr and R. G. Pearson, *J. Am. Chem. Soc*., 1983, **105**, 7512–7516.
44 P. Geerlings, F. D. Proft, W. Langenaeker, *Chem. Rev*. 2003, **103**, 1793-1874.
45 R. G. Pearson, *J. Org. Chem*., 1989, **54**, 1430–1432.
46 R. G. Parr, W. Yang, *J. Am. Chem. Soc*., 1984, **106**, 4049–4050.
47 J.A. Padron, R. Carasco, R.F. Pellon, *J. Pharm. Pharm. Sci*., 2002, **5**, 258-266.
48 R.P. Verma, A. Kurup, C. Hansch, *Bioorg Med. Chem*., 2005, **13** 237-255.
49 A.E. Reed, L.A. Curtiss, F. Weinhold, *Chem. Rev*., 1988, **88**, 899-926.
50 E. Espinosa, E. Molins, C. Lecomte, *ChemPhysLett*., 1998, **285**, 170–173.
51 V. R. Vangala, Pui Shan Chow, Reginald B. H. Tan, *Cryst. Growth Des*., 2012, **12**, 5925-5938.
52 S. Boys, F. Bernardi, *Mol. Phys*., 1970, **19**, 553–566.
53 J. M. L. Martin, J. El-Yazal, Jean-Pierre Francois, *J. Phys. Chem*., 1996, **100**, 15358-15367.
54 Editor: Russell D. Johnson, NIST Computational Chemistry Comparison and Benchmark Database, NIST Standard Reference Database, 2011, **15b**, http://cccbdb.nist.gov/
55 U. Koch, P. L. A. Popelier, *J PhysChem A*., 1995, **99**, 9747–9754.
56 I. Rozas, I. Alkorta, J. Elguero, *J Am Chem Soc.*, 2000, **122**, 11154-11161.
57 F. Biegler-Konig, J. Schonbohm, D. Bayles, *J. Comp. Chem*., 2001, **22**, 545-559.
58 S. Radhakrishnan, R. Parthsarathi, V. Subramanian, N. Somnathan, *Comput.Mater. Sci*., 2006, **37**, 318–322.
59 P.W. Atkins, Physical Chemistry, *Oxford University Press*, Oxford, 2001.
60 A. Shukla, E. Khan, P. Tandon, K. Sinha, *Journal of Molecular Structure*, 2017, **1131**, 225-235.
61 A. K. Ghose, V. N. Viswanadhan, J. J. Wendoloskl, *J. Comb. Chem*., 1999, **1**, 55-68.

† Electronic Supplementary Information

Study of hydrogen bonding interactions and chemical reactivity analysis of nitrofurantoin –3-aminobenzoic acid cocrystal using quantum chemical and spectroscopic (IR, Raman, ^{13}C SS-NMR) approach

Anuradha Shukla[a], Eram Khan[a], Karnica Srivastava[a], Kirti Sinha[a], Poonam Tandon[a*], Venu R. Vangala[b*]

[a]*Department of Physics, University of Lucknow, Lucknow 226007, Uttar Pradesh, India*

[b]*Centre for Pharmaceutical Engineering Science, School of Pharmacy and Medical Sciences, University of Bradford, Bradford BD7 1DP, United Kingdom*

Part I. FIGURES

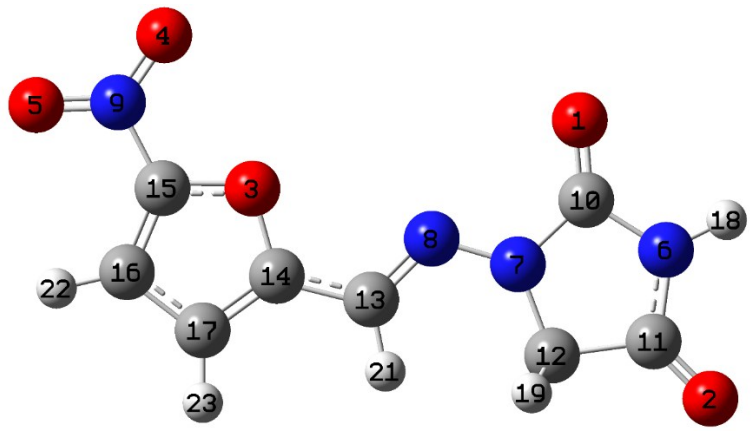

Fig. S1 Optimized structure for NF using wB97X-D/cc-pvTZ method and the atom numbering scheme adopted in this study.

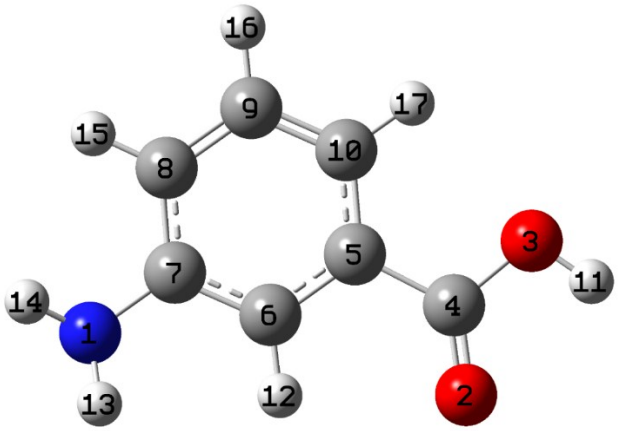

Fig. S2 Optimized structure for 3ABA using wB97X-D/cc-pvTZ method and the atom numbering scheme adopted in this study.

Vibrational assignments

NF-3ABA has hydrogen bonding that is reflected in both calculated IR and Raman spectra. To understand the effect of hydrogen bonding on IR and Raman spectra, we selected NH, OH and C=O stretching modes, as these bonds are involved in hydrogen bonding in the NF-3ABA. Calculated infrared spectra of NF-3ABA, NF and 3ABA which comprise of N-H, C=O and O-H stretching frequencies are shown in Fig. S7 (ESI†). The wavenumbers calculated using B3LYP/cc-pvTZ is given in the parenthesis.

Carbonyl group (C=O) vibrations are characteristic bands in vibrational spectra and for this reason; these types of bands have been subject of extensive studies.[1,2] The carbonyl compounds give rise to strong bands in the region 1870-1650 cm^{-1}.[3] The C16=O stretching mode is observed as medium band at 1827 cm^{-1} in the IR spectrum and calculated as medium intensity band at 1837 (1808) cm^{-1}. The C12=O stretching mode is observed as medium band at 1788 cm^{-1} in the IR spectrum and strong band at 1776 cm^{-1} in the Raman spectrum, however, it is calculated as medium intensity band at 1751 (1722) cm^{-1}, which matches well with the value calculated using wB97X-D/cc-pvTZ. The same mode is calculated at 1798 (1771) cm^{-1} for NF (API) and observed at 1782 cm^{-1} in the IR spectrum of NF. The unusual lowering of the carbonyl stretching wavenumber is also contributed to the electron releasing effect of the C=O bond due to intra-molecular charge transfer, as reported earlier[4] in addition to the intermolecular effect. This shift is clearly shown in the Fig. S7.

The position of N-H stretching band is dependent on the strength of hydrogen bond formed. In the observed FT-IR spectrum of NF-3ABA, the N5-H stretch is observed as a medium peak at 3150 cm^{-1} in the IR spectrum and at 3151 cm^{-1} in the Raman spectrum of NF-3ABA, whereas it is calculated as 3153 (3124) cm^{-1}, which matches well with the value calculated using wB97X-D/cc-pvTZ level of theory. The same mode is calculated at 3516 (3503) cm^{-1} and observed at 3287 cm^{-1} in the IR spectrum of NF. The N-H of Ring 2 is hydrogen bonded with C=O bond of carboxylic acid attached to the Ring 3 and the lowering of NH stretching wavenumber can be endorsed to the intermolecular N-H···O interaction.[5] This lowering in the wavenumber from NF to NF-3ABA is clearly shown in the Fig. S7.

The stretching vibration C34=O27 is calculated to be 1693 (1660) cm^{-1} and corresponds to the peak at 1688 cm^{-1}/ 1686 cm^{-1} in IR/Raman spectrum, which matches well with the value calculated using wB97X-D/cc-pvTZ level of theory. The same mode is calculated at 1757 (1725) cm^{-1} and observed at 1751 cm^{-1}/ 1696 cm^{-1} in the IR/Raman spectrum of 3-ABA. The lowering of wavenumber (as shown in Fig. S7) is due to presence of hydrogen bond in the NF-3ABA. The non-hydrogen bonded (free) hydroxyl group absorbs strongly in the region 3700-3584 cm^{-1}. Whereas the existence of hydrogen bond can lower the O-H stretching frequency to the 3550-3200 cm^{-1} region with increase in intensity and breadth.[6,7] The IR spectrum in the high wavenumber region shows a broad band at 3200 cm^{-1} and at 3216 cm^{-1} in the Raman spectrum attributed to hydrogen bonded OH stretching vibrations, whereas it is calculated at 3252 (3218) cm^{-1} in the case of NF-3ABA. The same mode is calculated at 3670 (3626) cm^{-1} in the case of 3ABA and observed at 3559 cm^{-1} in the IR spectra. This confirms that the OH group participate in intermolecular hydrogen bonding with a neighbouring molecule. The OH deformation mode appears as medium peak at 1400 cm^{-1}/1399 cm^{-1} in the IR/Raman spectrum whereas it is calculated at 1405 (1396) cm^{-1}.

References-

1 N. B. Colthup, L. H. Daly, S. E. Wiberley, *Academic Press*, New York, 1990, 3rd Eds., 289-325.
2 G. Socrates, *Wiley*, New York, 1980, 3rd Eds.
3 J. B. Lambert, H. F. Shurvell, R. G. Cooks, *Macmillan Publ*., New York, 1987.
4 J. Clarkson, W. E. Smith, *J. Mol. Struct*., 2003, **655**, 413-422.
5 D. Sajan, H.J. Ravindra, N. Mishra, I.H. Joe, *Vib. Spectrosc*., 2010, **54**, 72–80.
6 B. Smith, *CRC Press*, Washington, DC, 1999.
7 R. M. Silverstein, F. X. Webster, *John Wiley & Sons Inc*., New York, 2003.

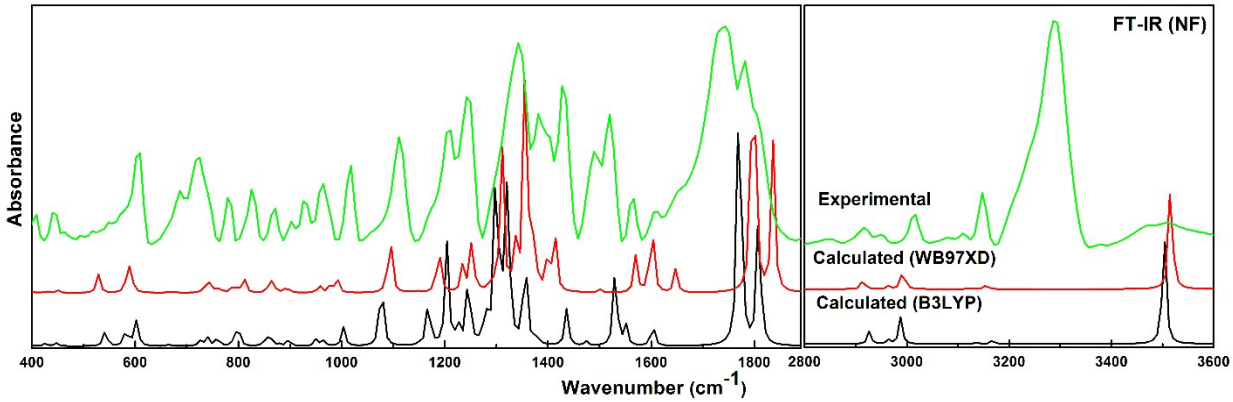

Fig. S3 Experimental and calculated FT-IR absorbance spectra of NF in the region, 400-3600 cm^{-1}.

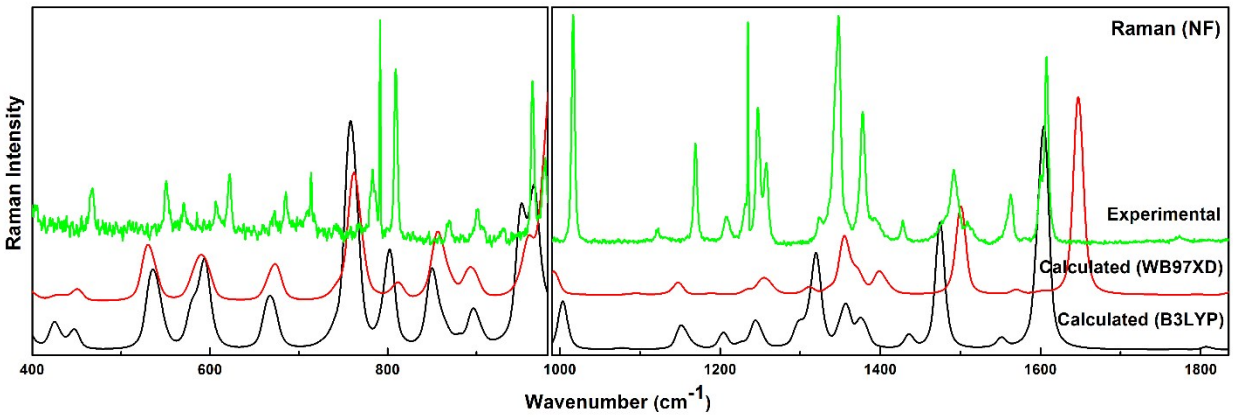

Fig. S4 Experimental and calculated Raman spectra of NF in the region, 400-1800 cm^{-1}.

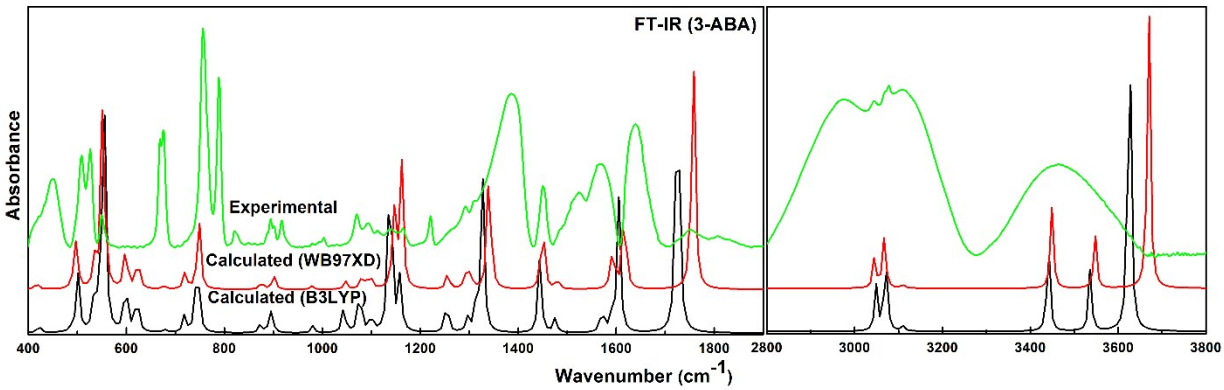

Fig. S5 Experimental and calculated FT-IR absorbance spectra of 3ABA in the region, 400-3800 cm^{-1}.

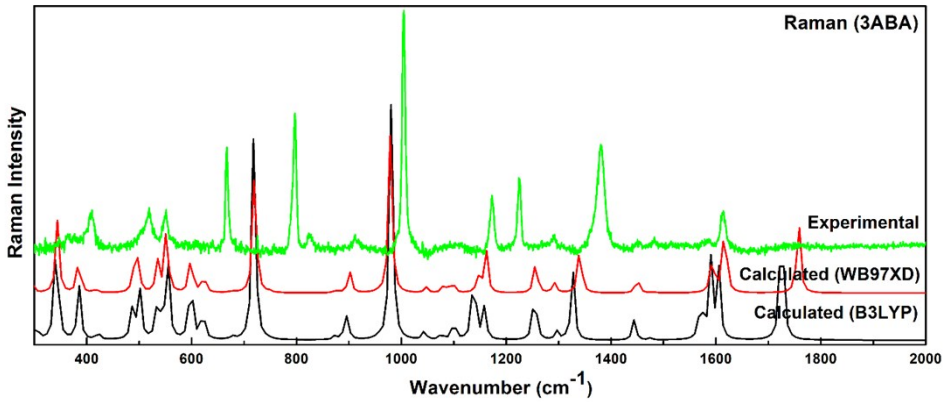

Fig. S6 Experimental and calculated Raman spectra of 3ABA in the region, 300-2000 cm^{-1}.

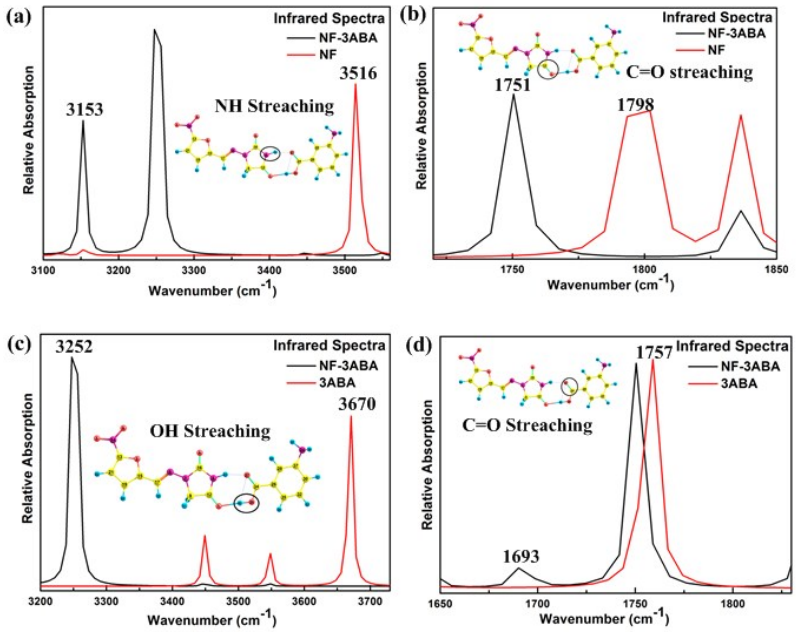

Fig. S7 Calculated infrared spectra of NF-3ABA, NF and 3ABA in the region of N-H, C=O and OH stretching using wB97X-D/cc-pvTZ level of theory.

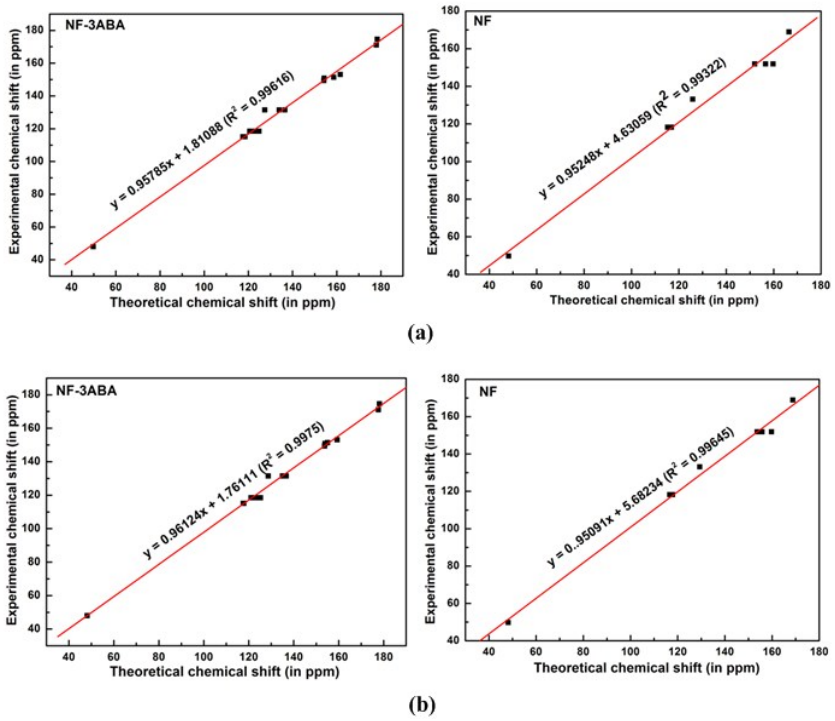

Fig. S8 ^{13}C NMR correlation graph of NF-3ABA and NF (a) using GIAO/B3LYP/cc-pVTZ. (b) GIAO/wB97X-D/cc-pVTZ

Reduced density gradient (RDG) and isosurface analysis

The multi-wavefunction analysis has been performed by reduced density gradient (RDG) plot and isosurface analysis of interactions to confirm the results obtain from the QTAIM analysis and the type of interactions present in the NF-3ABA. For this, initially the cube files were generated for the real spatial functions $\lambda_2\rho$ (the product of second largest eigen value of Hessian matrix and electron density) and RDG by Multiwfn software. Furthermore, we have plotted a scatter graph with isosurface value of about 0.5 a.u by taking $\lambda_2\rho$ in x-axis and RDG in y-axis as shown in Fig. S9 (ESI†). Each point in the graph corresponds to the critical points in AIM theory. If a horizontal line is drawn to the specified isosurface value (0.5 a.u), then the points crossing the line correspond to the RDG isosurfaces. It is seen from the graph that there are spike shaped collection of points in the region from –0.045 to 0.030 a.u and based on the value of $\lambda_2\rho$, the strength of the interactions were distinguished. In the figure shown, the points enclosed in the blue box correspond to hydrogen bonding interactions, the points enclosed in green box represent van der Waals interactions and the points enclosed in red box represent steric effect. Steric effect also has been observed where the ring is formed via hydrogen bonds. The isosurface density map for the non-bonded interactions is shown in Fig. S10 (ESI†), which indicates steric effect by red in colour and van der Waals interactions in dark green and hydrogen bond by blue in colour. From isosurface plot, the bond between imide NH, C=O of NF and acid C=O and -OH group in 3ABA is hydrogen bonded and represent by dark blue in colour showing its moderate nature.

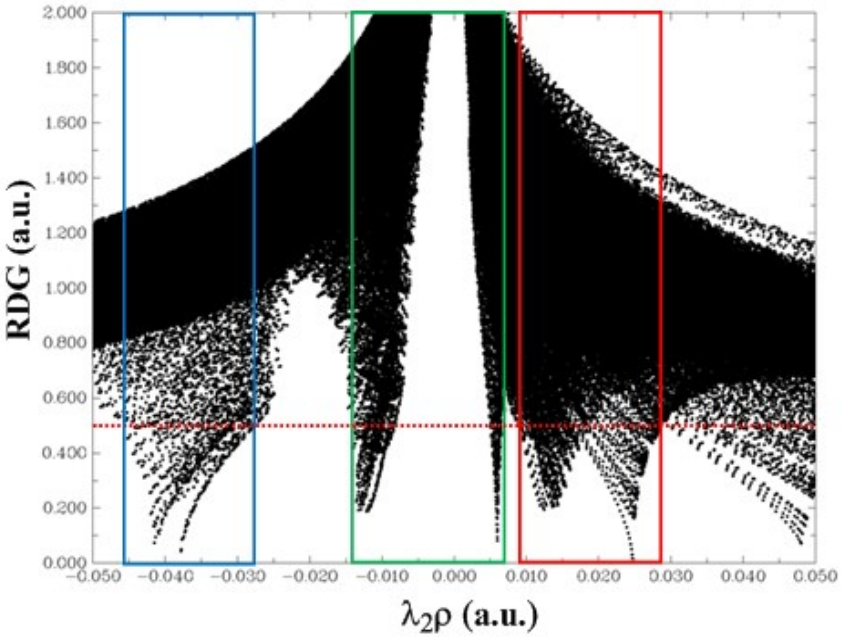

Fig. S9 Reduced density gradient plot of NF-3ABA.

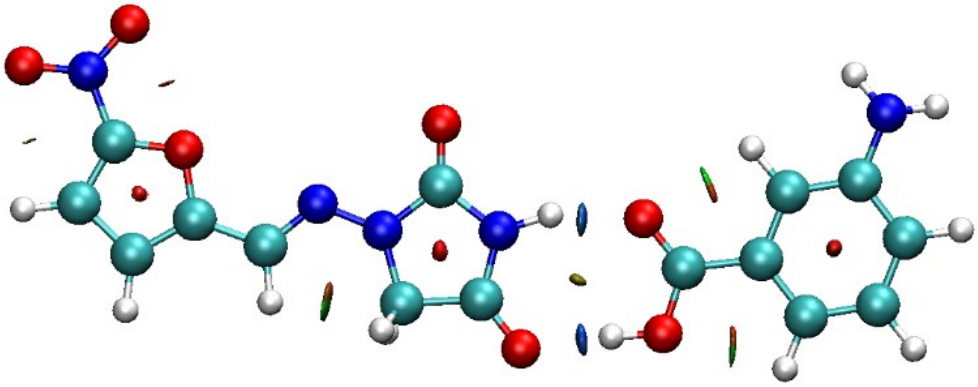

Fig. S10 Isosurface plot validating the presence of hydrogen bond, sterik effect and van der Waals interactions between the non-bonded atoms of NF-3ABA.

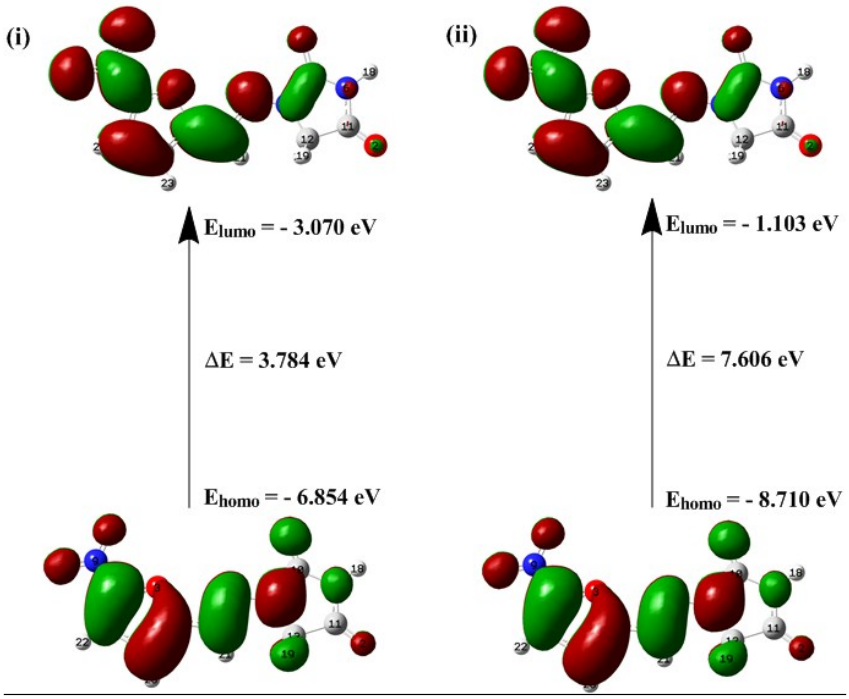

Fig. S11 HOMO-LUMO plot of NF with orbitals involved in electronic transitions in isolated (gaseous) phase (i) using wB97X-D/cc-pvTZ method (ii) using B3LYP/cc-pvTZ method.

Molecular electrostatic potential map of NF-3ABA

The molecular electrostatic potential (MEP) gives a pictorial method to recognize the relative polarity of the molecule. It can be used to analyse the electrophilic and the nucleophilic sites within the molecule where chemical reactions are likely to take place. The electrostatic potential is computed by creating an electrostatic potential grid. The different values of the electrostatic potential at the MEP surface are represented by different colours; red, electron rich; blue, electron deficient; light blue, slightly electron deficient region; yellow, slightly electron rich region; green, neutral; respectively.

The total electron density and electrostatic potential surface (ESP) of the molecules under investigation are constructed by using wB97X-D/cc-pvTZ method. The total electron density mapped with electrostatic potential surface of NF-3ABA is shown in Fig. S12. This orientation visibly show electrophilic region visible as red blob is localized over the NO_2 and carbonyl group attached to the ring R1 and R2 of the molecule respectively. In addition, a less negative area reflected as a yellowish blob is visible mainly over the oxygen atoms of carboxylic group attached to the ring R3 and a more nucleophilic region localised on the NH_2 and CH_2 group and is reflected as a bluish blob.

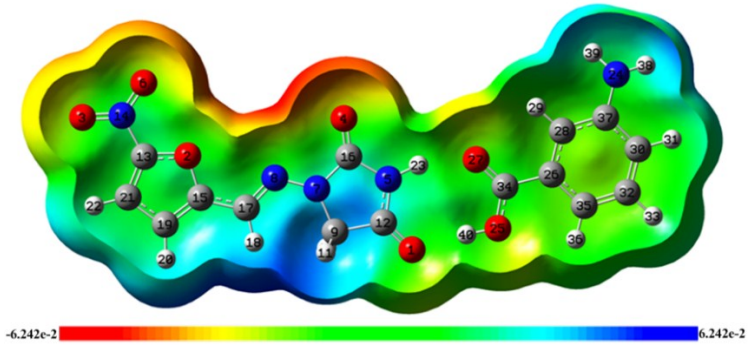

Fig. S12 Molecular electrostatic potential (MEP) formed using wB97X-D/cc-pvTZ method by mapping total density over electrostatic potential in gas phase for NF-3ABA cocrystal.

Part II. TABLES

Table S1 Comparison of geometrical parameters of NF and NF – 3-ABA.

Geometrical Parameters	Experimental		Calculated Optimized Parameters			
	NF-3ABA	NF	NF-3ABA		NF	
			B3LYP/ cc-pvTZ	wB97X-D/ cc-pvTZ	B3LYP/ cc-pvTZ	wB97X-D/ cc-pvTZ
Bond-Lengths (Å)						
O1-C12	1.2265	1.2063	1.2185	1.2138	1.2023	1.1976
O1-H40	1.8004	-	1.7567	1.7393	-	-
O2-C13	1.3524	1.3477	1.3478	1.3366	1.3476	1.3365
O2-C15	1.3722	1.3687	1.3581	1.3471	1.3582	1.3470
O3-N14	1.2297	1.2285	1.2278	1.2168	1.2276	1.2167
O4-C16	1.2042	1.1949	1.1938	1.1895	1.1954	1.1912
N5-C12	1.3573	1.3531	1.3534	1.3491	1.3744	1.3706
N5-C16	1.4038	1.3966	1.4058	1.4014	1.4041	1.3991
N5-H23	0.9443	0.9205	1.0297	1.0277	1.0076	1.0053
O6-N14	1.2369	1.2143	1.2202	1.2097	1.2200	1.2098
N7-N8	1.3589	1.3626	1.3359	1.3348	1.3376	1.3359
N7-C9	1.4484	1.4473	1.454	1.4438	1.4560	1.4456
N7-C16	1.3779	1.373	1.4062	1.3974	1.4012	1.3919
N8-C17	1.2877	1.2803	1.2826	1.2741	1.2824	1.2741
C9-H10	0.99	0.9301	1.0927	1.0924	1.0924	1.0925
C9-H11	0.9897	0.9856	1.0927	1.0924	1.0925	1.0923
C9-C12	1.5046	1.5041	1.5205	1.5157	1.5270	1.5224
C13-N14	1.4205	1.4113	1.4313	1.4341	1.4317	1.4347
C13-C21	1.3488	1.3391	1.3617	1.3537	1.3617	1.3537
C15-C17	1.4426	1.4369	1.4387	1.4449	1.4388	1.4445
C15-C19	1.3654	1.3526	1.3753	1.3659	1.3751	1.3658
C17-H18	0.9499	0.9887	1.0888	1.0888	1.0887	1.0888
C19-H20	0.9499	0.9264	1.0763	1.0761	1.0763	1.0765
C19-C21	1.4152	1.3985	1.414	1.4161	1.4141	1.4167
C21-H22	0.9503	0.9226	1.0744	1.0743	1.0743	1.0749
H23-O27	1.9059	-	1.7917	1.7766	-	-
N24-C37	1.3763	-	1.3907	1.388	-	-
N24-H38	0.8913	-	1.0067	1.0051	-	-
N24-H39	0.8831	-	1.0069	1.0053	-	-
O25-C34	1.3334	-	1.3284	1.3183	-	-
O25-H40	0.9024	-	0.989	0.985	-	-
C26-C28	1.3922	-	1.3927	1.3876	-	-
C26-C34	1.4832	-	1.4856	1.4867	-	-
C26-C35	1.3963	-	1.3958	1.3901	-	-
O27-C34	1.2228	-	1.2238	1.2184	-	-
C28-H29	0.9495	-	1.0815	1.0817	-	-
C28-C37	1.4039	-	1.3959	1.392	-	-
C30-H31	0.95	-	1.0832	1.0831	-	-
C30-C32	1.3901	-	1.3869	1.3832	-	-
C30-C37	1.4035	-	1.4015	1.3965	-	-
C32-H33	0.9496	-	1.0818	1.0814	-	-
C32-C35	1.3959	-	1.3881	1.3848	-	-
C35-H36	0.9501	-	1.0784	1.0787	-	-
Bond-Angles (°)						
C12-O1-H40	123.459	-	120.9708	120.6674	-	-
C13-O2-C15	104.6488	104.8201	106.1545	105.9937	106.1501	105.9294
C12-N5-C16	112.7266	113.0228	113.7052	113.456	114.5001	114.2805
C12-N5-H23	121.2363	118.9309	121.4627	121.4826	124.0161	124.1176
C16-N5-H23	125.9011	127.9628	124.8322	125.0612	121.4838	121.6019
N8-N7-C9	126.9954	127.5844	127.7022	127.3279	127.7318	127.0256
N8-N7-C16	119.961	119.2865	120.1369	120.1792	119.8737	120.2185
C9-N7-C16	113.0432	112.7821	112.1608	112.4905	112.3945	112.7556

N7-N8-C17	116.2641	116.9209	119.2374	118.8607	119.1684	118.4241
N7-C9-H10	111.4725	110.1039	112.6891	112.722	112.4628	112.2900
N7-C9-H11	111.4709	108.3285	112.693	112.7753	112.4603	112.2684
N7-C9-C12	101.5498	101.6822	102.095	101.9351	102.8274	102.6677
H10-C9-H11	109.2916	114.8676	108.7025	108.9873	108.7933	109.0524
H10-C9-C12	111.4333	110.0802	110.2656	110.118	110.0875	110.2119
H11-C9-C12	111.477	110.9542	110.2628	110.1251	110.0899	110.2178
O1-C12-N5	126.5515	125.7485	127.3776	127.3319	127.5339	127.4732
O1-C12-C9	125.8732	127.0593	125.4381	125.4006	126.8962	126.9288
N5-C12-C9	107.55	107.1909	107.1843	107.2675	105.5698	105.5980
O2-C13-N14	114.6736	116.1495	117.7268	117.4979	117.6940	117.6787
O2-C13-C21	113.2776	113.0483	112.0792	112.5713	112.0877	112.6090
N14-C13-C21	132.0367	130.8022	130.194	129.9307	130.2183	129.7123
O3-N14-O6	124.1922	124.2619	126.1782	126.3585	126.2021	126.3634
O3-N14-C13	117.3027	117.4108	115.688	115.6197	115.6901	115.5733
O6-N14-C13	118.5007	118.3036	118.1337	118.0217	118.1078	118.0633
O2-C15-C17	117.7588	117.7624	119.8985	119.495	119.8172	119.642
O2-C15-C19	110.3699	109.6004	109.9942	110.4273	110.0025	110.5235
C17-C15-C19	131.8676	132.6225	130.1074	130.0777	130.1803	129.8344
O4-C16-N5	126.7129	126.6982	127.0092	126.9831	126.6614	126.5916
N8-C16-N7	128.2102	119.2865	128.1361	128.1664	119.8737	120.2185
N5-C16-N7	105.0768	105.2273	104.8547	104.8505	104.7082	104.6983
N8-C17-C15	119.474	119.0128	121.3508	120.811	121.2521	120.9265
N8-C17-H18	120.2754	126.0008	123.7601	124.1218	123.7857	123.9358
C15-C17-H18	120.2505	114.8383	114.8891	115.0672	114.9622	115.1376
C15-C19-H20	126.5221	121.4467	126.0529	126.1371	126.0786	126.0977
C15-C19-C21	106.9286	107.8642	106.7012	106.3962	106.6959	106.3187
H20-C19-C21	126.5493	130.6543	127.2458	127.4666	127.2255	127.5836
C13-C21-C19	104.768	104.6656	105.0709	104.6116	105.0638	104.6194
C13-C21-H22	127.6111	122.5127	125.9686	126.1239	126.0010	125.8516
C19-C21-H22	127.6209	132.7174	128.9605	129.2645	128.9352	129.5290
N5-H23-O27	157.9922	-	160.4478	160.6013	-	-
C37-N24-H38	118.1809	-	115.7955	115.5284	-	-
C37-N24-H39	120.7994	-	115.6535	115.3968	-	-
H38-N24-H39	118.6861	-	112.4012	112.3728	-	-
C34-O25-H40	107.7043	-	110.8117	110.8734	-	-
C28-C26-C34	116.8926	-	117.9153	117.8286	-	-
C28-C26-C35	121.058	-	120.5841	120.7937	-	-
C34-C26-C35	122.0484	-	121.5004	121.3771	-	-
H23-O27-C34	133.5836	-	131.7077	131.2132	-	-
C26-C28-H29	119.7716	-	118.7502	118.9412	-	-
C26-C28-C37	120.5158	-	120.677	120.5197	-	-
H29-C28-C37	119.7126	-	120.5727	120.5391	-	-
H31-C30-C32	119.4935	-	119.9019	119.8586	-	-
H31-C30-C37	119.5035	-	119.3914	119.4238	-	-
C32-C30-C37	121.003	-	120.706	120.717	-	-
C30-C32-H33	119.6468	-	119.3045	119.392	-	-
C30-C32-C35	120.6824	-	120.8806	120.8281	-	-
H33-C32-C35	119.6708	-	119.8149	119.7799	-	-
O25-C34-C26	114.4729	-	114.0079	113.9856	-	-
O25-C34-O27	122.4903	-	123.2221	123.455	-	-
C26-C34-O27	123.0369	-	122.77	122.5594	-	-
C26-C35-C32	118.5739	-	118.7904	118.7149	-	-
C26-C35-H36	120.6938	-	120.1354	120.2943	-	-
C32-C35-H36	120.7323	-	121.0741	120.9907	-	-
N24-C37-C28	120.3602	-	120.7975	120.7236	-	-
N24-C37-C30	121.4112	-	120.7773	120.7944	-	-
C28-C37-C30	118.1533	-	118.3619	118.4266	-	-
Dihedral-Angles (°)						
H40-O1-C12-N5	-2.2199	-	-0.1869	-0.9852	-	-
H40-O1-C12-C9	179.8419	-	179.784	178.9543	-	-
C12-O1-O25-C34	-2.7729	-	0.3716	1.7338	-	-

C15-O2-C13-N14	-179.749	-179.877	-179.9766	-179.9213	179.9624	179.987
C15-O2-C13-C21	-0.8596	0.1232	-0.0059	-0.0011	0.0047	0.0004
C13-O2-C15-C17	-178.616	-178.6492	179.9997	179.9598	179.9922	-179.9993
C13-O2-C15-C19	0.7777	0.1285	-0.0025	0.0157	0.0013	-0.0055
C16-N5-C12-O1	-179.739	-178.5668	179.8948	179.7283	-179.982	-179.9636
C16-N5-C12-C9	-1.4909	1.8169	-0.0805	-0.22	0.0027	0.0230
H23-N5-C12-O1	4.2609	4.4936	-0.0704	-0.1439	0.0256	-0.0794
H23-N5-C12-C9	-177.491	-175.1227	179.9543	179.9078	-179.9897	179.9071
C12-N5-C16-O4	-179.826	176.926	-179.9235	-179.7865	179.9988	179.9319
C12-N5-C16-N7	0.0781	-3.0362	0.0749	0.1942	-0.0095	-0.0392
H23-N5-C16-O4	-4.0486	-6.4717	0.0403	0.0804	-0.0086	0.0446
H23-N5-C16-N7	175.8558	173.5661	-179.9612	-179.939	179.9831	-179.9266
C12-N5-H23-O27	-2.7022	-	0.2127	0.5513	-	-
C16-N5-H23-O27	-178.147	-	-179.7485	-179.3054	-	-
C9-N7-N8-C17	-3.0811	-7.0713	0.1068	0.5546	-0.032	-0.122
C16-N7-N8-C17	177.1832	-179.7879	180.0046	179.9376	180.008	-179.9171
N8-N7-C9-H10	59.2325	68.1898	61.6334	61.3752	61.6470	61.8155
N8-N7-C9-H11	-63.1934	-58.1799	-61.8394	-62.5687	-61.5926	-61.4889
N8-N7-C9-C12	177.9945	-175.1289	179.8977	179.3867	-179.9737	-179.835
C16-N7-C9-H10	-121.016	-118.6982	-118.2712	-118.0475	-118.3905	-118.3765
C16-N7-C9-H11	116.5578	114.9321	118.256	118.0086	118.3699	118.3192
C16-N7-C9-C12	-2.2543	-2.017	-0.0069	-0.0359	-0.0112	-0.0269
N8-N7-C16-O4	1.1475	-3.1289	0.0482	0.426	-0.0299	-0.1075
N8-N7-C16-N5	-178.755	176.8326	-179.9502	-179.5543	179.9786	179.8629
C9-N7-C16-O4	-178.623	-176.8731	179.9609	179.895	-179.9957	-179.9302
C9-N7-C16-N5	1.4744	3.0883	-0.0375	-0.0854	0.0128	0.0402
N7-N8-C17-C15	-179.664	-179.7651	-179.9989	-179.8827	-180.0045	179.9881
N7-N8-C17-H18	0.3191	4.9006	0.0234	0.1322	0.0039	-0.0217
N7-C9-C12-O1	-179.562	-179.5106	-179.925	-179.8001	-180.0102	-180.011
N7-C9-C12-N5	2.1747	0.0992	0.0508	0.1495	0.0049	0.0023
H10-C9-C12-O1	-60.7723	-62.8121	-59.9488	-59.9406	-59.9762	-60.208
H10-C9-C12-N5	120.9647	116.7978	120.027	120.009	120.039	119.8054
H11-C9-C12-O1	61.6298	65.4629	60.0956	60.2755	59.9576	60.2085
H11-C9-C12-N5	-116.633	-114.9273	-119.9286	-119.7749	-120.0272	-119.7782
O2-C13-N14-O3	-176.641	-175.8332	-179.9757	179.9895	179.9138	179.9834
O2-C13-N14-O6	4.0944	5.8609	0.0292	0.0037	-0.0869	-0.0308
C21-C13-N14-O3	4.7331	4.1666	0.0598	0.0857	-0.1376	-0.0328
C21-C13-N14-O6	-174.532	-174.1392	-179.9352	-179.9002	179.8617	179.9531
O2-C13-C21-C19	0.5988	-0.311	0.0115	-0.0129	-0.0086	0.0045
O2-C13-C21-H22	-179.354	-177.0324	179.9995	-179.979	-179.9951	179.9904
N14-C13-C21-C19	179.24	179.6891	179.9775	179.8947	-179.9595	-179.98
N14-C13-C21-H22	-0.713	2.9678	-0.0344	-0.0714	0.054	0.0059
O2-C15-C17-N8	-4.5418	-0.5219	0.0424	0.4342	0.024	-0.0591
O2-C15-C17-H18	175.4746	175.3196	-179.978	-179.5795	180.0163	179.9499
C19-C15-C17-N8	176.2215	-178.957	-179.9549	-179.6343	180.0129	179.9485
C19-C15-C17-H18	-3.7622	-3.1154	0.0247	0.3521	0.0051	-0.0425
O2-C15-C19-H20	179.6014	-178.3909	-179.994	-179.9695	-179.9989	179.9925
O2-C15-C19-C21	-0.4412	-0.3191	0.0094	-0.0235	-0.0065	0.0082
C17-C15-C19-H20	-1.1191	0.1391	0.0036	0.0941	0.0114	-0.0145
C17-C15-C19-C21	178.8383	178.211	180.007	-179.96	-179.9962	180.0012
C15-C19-C21-C13	-0.0825	0.376	-0.0124	0.0216	0.0089	-0.0075
C15-C19-C21-H22	179.8705	176.6122	-180.0	179.9862	179.9949	-179.9927
H20-C19-C21-C13	179.8749	178.2077	-180.0089	179.9666	180.0012	-179.9915
H20-C19-C21-H22	-0.1721	-5.5561	0.0035	-0.0688	-0.0128	0.0233
N5-H23-O27-C34	-0.7293	-	0.3074	1.4738	-	-
H38-N24-C37-C28	-175.370	-	-157.4365	-156.996	-	-
H38-N24-C37-C30	7.8432	-	25.5058	25.753	-	-
H39-N24-C37-C28	-12.9401	-	-22.8749	-23.074	-	-
H39-N24-C37-C30	170.2733	-	160.0674	159.6749	-	-
H40-O25-C34-C26	-176.647	-	-179.9803	179.9242	-	-
H40-O25-C34-O27	3.3397	-	-0.0161	-0.122	-	-
C34-C26-C28-H29	-1.223	-	0.3243	0.349	-	-

C34-C26-C28-C37	178.7821	-	-179.823	-179.743	-	-
C35-C26-C28-H29	179.1177	-	-179.8449	-179.9248	-	-
C35-C26-C28-C37	-0.8771	-	0.0077	-0.0168	-	-
C28-C26-C34-O25	-177.968	-	-179.4364	-178.8927	-	-
C28-C26-C34-O27	2.0446	-	0.5993	1.153	-	-
C35-C26-C34-O25	1.6874	-	0.7345	1.3828	-	-
C35-C26-C34-O27	-178.299	-	-179.2298	-178.5715	-	-
C28-C26-C35-C32	0.6009	-	-0.072	-0.0482	-	-
C28-C26-C35-H36	-179.382	-	-179.9607	-179.8988	-	-
C34-C26-C35-C32	-179.040	-	179.7525	179.6681	-	-
C34-C26-C35-H36	0.9759	-	-0.1362	-0.1825	-	-
H23-O27-C34-O25	-1.1824	-	-0.4064	-1.4865	-	-
H23-O27-C34-C26	178.803	-	179.5547	178.4635	-	-
C26-C28-C37-N24	-176.786	-	-177.0966	-177.2727	-	-
C26-C28-C37-C30	0.1033	-	0.0307	0.0422	-	-
H29-C28-C37-N24	3.2188	-	2.7533	2.6339	-	-
H29-C28-C37-C30	-179.891	-	179.8806	179.9488	-	-
H31-C30-C32-H33	-1.2772	-	-0.3751	-0.3141	-	-
H31-C30-C32-C35	178.7432	-	179.6389	179.6393	-	-
C37-C30-C32-H33	178.7532	-	179.9246	179.9834	-	-
C37-C30-C32-C35	-1.2264	-	-0.0614	-0.0632	-	-
H31-C30-C37-N24	-2.1762	-	-2.5782	-2.3936	-	-
H31-C30-C37-C28	-179.031	-	-179.7061	-179.7066	-	-
C32-C30-C37-N24	177.7934	-	177.1236	177.3101	-	-
C32-C30-C37-C28	0.9381	-	-0.0043	-0.0028	-	-
C30-C32-C35-C26	0.4432	-	0.0988	0.0879	-	-
C30-C32-C35-H36	-179.573	-	179.9864	179.9374	-	-
H33-C32-C35-C26	-179.536	-	-179.8871	-179.9588	-	-
H33-C32-C35-H36	0.4471	-	0.0005	-0.1093	-	-

Table S2 Theoretical and experimental vibrational wavenumbers (in cm^{-1}) of NF-3ABA and their assignments using wB97X-D/cc-pvTZ level of theory.

Calculated		Experimental		Potential Energy Distribution (≥5%)
Unscaled	Scaled	IR	Raman	
3710	3547	3470	3471	R3[$v_a(NH_2)$](98)
3608	3449	3362	3363	R3[$v_s(NH_2)$](98)
3401	3252	3200	3216	v(O25H)(89)+R2[v(N5H)](7)
3304	3159			R1[v(CH)](99)
3298	3153	3150	3151	R2[v(N5H)](88)+v(O25H)(8)
3280	3136	3134	3135	R1[v(CH)](99)
3247	3104	3119	3119	R3[v(CH)](99)
3216	3074	3093	3100	R3[v(CH)](97)
3214	3072	3063		R3[v(CH)](99)
3185	3045	3049		R3[v(CH)](99)
3125	2988	3010		v(C17H)(99)
3101	2965	2961	2959	R2[$v_a(CH_2)$](100)
3055	2921	2918	2924	R2[$v_s(CH_2)$](99)
1922	1837	1827		R2[v(C16=O)(75)+v(NC)(11)]
1832	1751	1788	1776	R2[v(C12=O)(64)+v(NC)(10)+v(C34=O)(5)
1771	1693	1688	1686	v(C34=O)(61)+v(O25C)(6)+δ(O25HC34)(6)+R3[v(C26C34)(5)+ρ(C34C) 5)]
1721	1646	1653		v(N8C)(59)+R1[v(C15C17)(14)+ρ(C17H)(13)+v(CC)(6)]
1692	1617	1620		R3[v(CC)(54)+δ(NH_2)](10)+v(N24C)(7)+δ_{in}(CH)(14)+δ_a(5)]
1675	1601			R1[$v_a(NO_2)$(77)+ρ(NO_2)(8)+v(CC)(7)
1666	1593	1603	1612	R3[δ(NH_2)(41)+v(CC)(37)+δ_{in}(C35H)(5)]
1661	1588	1583		R3[δ(NH_2)](38)+v(CC)(39)+δ_{in}(C30H)(5)+δ'_a(5)]
1643	1571	1562	1566	R1[v(CC)(56)+$v_a(NO_2)$(15)+δ_{in}(CH)(10)]+v(N8C)(8)
1570	1500	1512	1512	R1[v(CC)(46)+δ_{ring}(13)+v(C15C17)(12)+v(C13N)(5)]+v(N8C)(6)
1551	1482	1491	1485	R3[δ_{in}(CH)(47)+(CC)(36)]
1519	1452	1464		R3[v(CC)(33)+δ_{in}(CH)](19)+v(N24C)(7)+v(C26C34)(6)+δ_{in}(C26C34)(6)]
1491	1426	1427	1437	R2[$\delta_{sci}(CH_2)$](83)
1470	1405	1400	1399	δ(O25HC34)(31)+v(O25C)(16)+R3[(δ(C34OO)(7)+v(C26C34)(5)]
1468	1403	1385	1382	R1[v(CO)(24)+v(C13N)(7)+v(CC)(11)]+δ(O25HC34)(7)

1444	1381			R2[δ_{in}(NH)(38)+ν(NC)(23)+ν(C12=O)(7)]
1434	1371	1367	1372	R1[ν_s(NO_2)(35)+ν(CC)(11)+δ(NO_2)(9)+ν(C13N)(7)]+R2[δ_{in}(NH)](12)
1421	1359			R2[ν(NC)(34)+δ_{in}(NH)(17)+δ_{in}(C12=O)(12)+ν(CC)(10)+δ'_{ring}(5)
1410	1348	1352	1344	R1[ρ(C17H)(20)+ν_s(NO_2)(12)+ν(CC)(7)]+R2[ν(NC)(10)+δ_{ring}(6)+ω(CH_2)(5)+ν(N7N8)(5)]
1374	1313	1319	1321	R2[ω(CH_2)(31)+ν(CC)(7)+δ_{ring}(6)+ν(NC)(8)+R1[ρ(C17H)](26)
1361	1302			R3[ν(CC)(78)+δ_{in}(CH)(25)]
1357	1298	1288	1289	R3[ν(N24C)(17)+δ_{in}(CH)(43)+ρ(NH_2)(7)+ν(CC)(6)+δ_{tring}(5)]+δ(O25HC34)(5)
1324	1266	1263	1264	R3[δ_{in}(CH)(36)+ν(N24C)(12)+δ_{tring}(7)+ν(CC)(7)+ν(C26C34)(7)+δ(O25HC34)(13)
1320	1262			R1[ν(CO)(31)+δ'_{ring}(7)+δ_{in}(CH)(6)]+R2[ν(NC)(12)+ν(N7N8)(10)+δ(N8C17N7)(5)]
1312	1255	1250	1252	R1[ν(CC)(29)+ν(C15C17)(9)+ν(C15O)(9)+δ_{in}(CH)(9)]+R2[ν(N7N8)(10)+ν(NC)(6)]
1302	1245	1238	1239	ν(O25C)(32)+δ(O25HC34)(24)+R3[ν(N24C)(10)+ν(C26C34)(5)+δ_{in}(CH)(5)]
1296	1239			R1[ν(C13O)(29)+ν(CC)(8)+δ'_{ring}(6)+ν(C13N)(6)+ν(C15O)(6)]+R2[ν(NC)(14)+ν(N7N8)(13)]
1252	1197	1219	1220	R2[ω(CH_2)(30)+ν(NC)(40)+ν(N7N8)(7)+δ_{ring}(5)]
1212	1158	1167	1176	R2[γ(CH_2)](96)
1206	1153			R3[δ_{in}(CH)(75)+ν(CC)(18)]
1202	1149			R1[δ_{in}(CH)(57)+ν(C13N)(9)+ν(C15C17)(5)+δ'_{ring}(5)]
1162	1111	1117	1117	R2[ν(NC)(55)+δ_{in}(C16=O)(9)+δ_{in}(NH)(8)+ν(N7N8)(6)]
1153	1103	1109		R3[δ_{in}(CH)(40)+ν(CC)(11)+ν(CC)(10)+ν(C26C34)(7)+ρ(NH_2)(6)]+ν(O25C)(9)
1139	1089	1067		R3[δ_{in}(CH)(30)+ρ(NH_2)(18)+ν(CC)(33)+ν(C26C34)(5)]
1096	1048	1026	1030	R3[ρ(NH_2)(45)+ν(CC)(37)+δ_{in}(CH)(8)]
1041	995	991	993	R1[δ_{in}(CH)(58)+ν(CC)(25)+ν(CO)(10)]
1027	982			R2[ρ(CH_2)(68)+oop(C12=O)(17)+τ(7)]
1025	980			R1[ν(CO)(42)+δ'_{ring}(14)+ν(C15C17)(10)+δ_{in}(CH)(6)]
1025	980	982	984	R3[δ_{tring}(63)+ν(CC)(34)]
1012	967			R3[oop(CH)(86)+puck(9)]
1002	958	966	968	R1[δ_{ring}(37)+ν(C13N)(10)+δ_{in}(CH)(14)+ν(CO)(11)+ν(CC)(12)]
954	912	920	921	R3[ν(CC)(25)+ν(N24C)(14)+ν(C26C34)(12)+δa(9)+δ_{in}(CH)(5)]+ν(O25C)(8)
941	899	912	912	R3[oop(CH)(67)+puck(13)+oop(C26C34)(7)]
938	897	885	887	R2[ν(CC)(56)+ν(NC)(13)+δ_{in}(C12=O)(6)+ω(CH_2)(5)]
932	891			R1[ω(C17H)(48)+oop(CH)(5)]+τ(N8C17)(21)+τ(O1H40)(6)
925	884	876		τ(O1H40)(48)+τ(O25H40)(32)+τ(O25C)(11)
916	876			R3[oop(CH)](72)+oop(C37N)(8)+puck(6)]
909	869			R1[oop(CH)(74)+τ(15)]
898	858	854		R2[δ(N8C17N7)(17)+ν(NC)(21)+δ'_{ring}(9)+ν(N7N8)(8)+R1[δ'_{ring}(15)+δ(C15C17N)(12)]
883	844	835		R2[oop(NH)(27)+τ(O1H40)(26)+τ(O27H)(21)+τ(O25H40)(18)+τ(O25C)(5)
849	812	810	812	R1[δ_{sci}(NO_2)(60)+δ'_{ring}(18)+δ_{ring}(9)]
836	799			R3[ω(C34C)(20)+oop(CH)(43)+puck(17)+oop(C26C34)(12)]
822	786	787		R1[oop(CH)(70)+τ'(9)+ω(N14C)(9)]
804	769	762	790	R2[ν(NC)(20)+δ'_{ring}(7)+δ_{in}(C16=O)(5)+δ_{ring}(5)]+R1[δ'_{ring}(16)+δ_{ring}(11)+ν(C15C17)(6)+(δ(C15C17N)(5)]
782	747	752	754	R3[ω(C34C)(21)+oop(CH)(29)+(δ(C34OO)(9)+oop(C37N)(9)]
781	747			R1[ω(N14C)(62)+oop(C13N)(12)+oop(CH)(18)+τ'(5)]
777	743	737	736	R3[(δ(C34OO)(20)+ω(C34C)(11)+oop(CH)(17)+δ_{tring}(6)+δ'_a(6)]+δ(O1O25C34)(6)
767	733			R2[oop(C16=O)(71)τ'(14)+τ(9)]
708	677	687	696	R1[τ'(39)+oop(C15C17)(33)+τ(21)]
705	674		664	R3[puck(66)+oop(C32H)(13)+oop(C37N)(13)+oop(C26C34)(5)]
705	674			R2[δ_{ring}(25)+δ'_{ring}(12)+δ_{in}(C16=O)(11)+ν(NC)(11)+δ_{in}(N7N)(9)+δ_{in}(C12=O)(6)]
679	650	656	655	R3[(δ(C34OO)(34)+δ_a(32)+δ'_a(12)]+δ(O1O25C34)(6)
641	613	625	629	R2[δ_{in}(C12=O)(22)+δ_{in}(C16=O)(15)+δ_{ring}(15)+δ_{in}(N7N)(10)+δ'_{ring}(9)+δ(N8C17N7)(6)]
621	593	609	608	R2[δ'_{ring}(33)+δ_{ring}(15)+ν(NC)(17)+ν(C12=O)(5)]
612	585			R1[τ(52)+τ'(24)+oop(C13N)(18)]
604	578		579	R2[oop(C12=O)(58)+ρ(CH_2)(16)+τ(13)+γ(CH_2)(7)]
588	563	573	570	R3[ω(N24C)(39)+oop(C37N)(17)+ν(N24C)(6)+τ'_a(6)+puck(5)+τ_a(5)+oop(C26C34)(5)]
570	545	550	550	R3[δ'_a(32)+ρ(C34C)(31)+δ_{in}(C26C34)(7)+δ_a(5)]
562	537			R1[ρ(NO_2)(43)+δ_{in}(C13N)(21)+δ_{in}(C15C17)(10)]+R2[δ(N8C17N7)](5)
535	511	511	514	R3[ω(N24C)(26)+oop(C37N)(19)+τ_a(13)+τ'_a(11)+oop(C26C34)(8)]
523	500	471	471	R3[δ'_a(18)+ω(N24C)(14)+ρ(C34C)(14)+ν(N24C)(13)+δ_{in}(C26C34)(10)+δ_{in}(C37N)(6)]
475	454	447	447	R2[δ(N8C17N7)(17)+δ_{in}(C12=O)(9)+δ_{in}(N7N)(5)]+R1[ν(C13N)(13)+ρ(NOO)(11)+δ_{in}(C15C17)(9)+δ_{ring}(5)+δ(NOO-)(5)]
458	438		431	R2[δ_{in}(C16=O)(16)+δ_{in}(C12=O)(12)]+R1[δ_{in}(C15C17)(11)+δ(C15C17N)(8)+ρ(NOO)(6)+ν(NC)(5)]
445	425		425	R3[τ_a(36)+τ'_a(32)+oop(C26C34)(14)+oop(C30H)(9)]
426	407	422		R1[ν(C13N)(21)+δ(NOO-)(8)+δ_{ring}(7)]+R2[δ_{in}(C12=O)(14)+δ_{in}(C16=O)(6)]
418	400		407	R3[δ_a(31)+δ_{in}(C37N)(21)+ν(C26C34)(13)+δ(C34OO)(6)]

393	376	-	38	τ(N8C17)(29)+R1[τ′(16)+τ(14)+oop(C15C17)(9)+ω(C17H)(8)+oop(C13N)(7)]+R2[oop(N7N)](7)
380	363	-		R3[δ_{in}(C37N)(38)+ρ(C34C)(16)+ν(C26C34)(9)+ν(CC)(6)]+ν(O1H40)(10)
310	296	-	302	R3[τ(N24C)](92)
297	284	-		R2[δ_{in}(N7N)(18)+ν(NC)(6)+δ_{in}(C16=O)(15)+δ(N8C17N7)(5)]+R1[δ_{in}(C13N)(12)+δ_{in}(C15C17)(10)+ρ(NOO)(6)+ν(C15C17)(6)]
294	281	-	260	R2[τ(N7N)(38)+oop(N7N)(21)+τ′(11)]+R1[τ(C15C17)(8)+oop(C15C17)(6)]+τ(N8C17)(5)
235	225	-	235	R3[δ_{in}(C26C34)(29)+δ_{in}(C37N)(8)]+δ(O1O25C34)(23)+ν(O27H23)(8)+R1[δ_{in}(C13N)](6)
232	221	-	231	R1[δ_{in}(C13N)(18)+ρ(NOO)(11)+δ(C15C17N)(7)+ν(C15C17)(5)]+ν(O1H40)(12)+R3[δ_{in}(C26C34)](11)
227	217	-	202	R3[τ'_a(44)+τ_a(24)+puck(11)+oop(CH)(13)]
204	195	-	187	R1[oop(C13N)(50)+oop(C15C17)(6)]+R2[τ(N7N)(13)+τ′(7)]+τ(N8C17)(5)
181	173	-	179	R2[τ′(69)+oop(N7N)(13)]
172	164	-		R2[τ′(15)+τ(15)+oop(NH)(8)]+R3[oop(C26C34)(15)+τ_a(11)+oop(C28H)(6)]+τ(O1H40)(10)+τ(O25C)(5)
168	161	-		ν(O1H40)(27)+δ(O1O25C34)(16)+R1[δ_{in}(C13N)](15)+R2[δ_{in}(N7N)(13)+δ(N8C17N7)(9)]
164	157	-	142	R2[τ(49)+oop(NH)(29)]+τ(O25H40)(6)
131	125	-	108	R2[oop(N7N)](24)+R1[oop(C13N)(18)+oop(C15C17)(14)+τ(C13N)(10)]
91	87	-	-	δ(O1O25C34)(35)+ν(O1H40)(22)+R1[δ_{in}(C15C17)](7)+ν(O27H23)(5)
88	84	-	-	ν(O27H23)(35)+δ(O1O25C34)(18)+δ(O25HC34)(13)+ν(O1H40)(12)
87	83	-	-	R1[τ(C13N)](27)+R2[oop(N7N)(23)+τ′(13)+oop(NH)(10)]+τ(O27H)(8)
68	65	-	-	τ(O25H40)(31)+R3[τ(C26C34)](28)+τ(O25C)(19)+τ(O27H)(12)
61	59	-	-	R1[τ(C13N)(32)+oop(C15C17)(6)]+R2[oop(NH)](13)+τ(O27H)(9)+τ(O1H40)(6)
60	57	-	-	ν(O27H23)(12)+R1[δin(C15C17)(11)+δ(C15C17N)(11)+τ(C13N)(5)]+δ(O1O25C34)(10)+ν(O1H40)(10)+R3[ρ(C34C)(9)+δin(C26C34)(7)]
38	36	-	-	τ(O1H40)22)+R2[oop(N7N)(16)+τ′(5)+R1[τ(C15C17)(14)+τ(C13N)(6)]+τ(O25H40)(13)+τ(O25C)(6)
26	25	-	-	τ(O25H40)(25)+R2[oop(N7N)](10)+R1[τ(C15C17)(7)+δ(C15C17N)(6)]+τ(O1H40)(6)+ν(O27H23)(6)
25	24	-	-	τ(O25H40)(22)+R2[oop(N7N)](9)+R1[τ(C15C17)(8)+δ(C15C17N)(7)+δ_{in}(C15C17)(5)]+ν(O27H23)(7)+τ(O1H40)(5)
13	13	-	-	τ(O27H)(23)+R3[τ(C26C34)](15)+τ(O25H40)(12)+τ(O25C)(12)+τ(O1H40)(7)+R2[τ(N7N)(6)+oop(NH)(5)]+R1[τ(C15C17)](6)
8	7	-	-	R1[τ(C15C17)](17)+τ(O1H40)(13)+R2[τ′(11)+oop(N7N)(10)+oop(NH)(7)]+τ(O25H40)(8)+τ(O27H)(5)+R3[τ(C26C34)](5)

Table S3 Theoretical and experimental vibrational wavenumbers (in cm^{-1}) of NF-3ABA and their assignments using B3LYP/cc-pvTZ level of theory.

Calculated		Experimental		Potential Energy Distribution (≥5%)
Unscaled	**Scaled**	**IR**	**Raman**	
3665	3537	3470	3471	R3[$\nu_a(NH_2)$](100)
3566	3441	3362	3363	R3[$\nu_s(NH_2)$](100)
3335	3218	3200	3216	ν(O25H)(88)+R2[ν(N5H)](7)
3281	3167			R1[ν(CH)](98)
3251	3138	3150	3151	R1[ν(CH)](99)
3237	3124	3134	3135	R2[ν(N5H)](87)+ν(O25H)(8)
3223	3110	3119	3119	R3[ν(CH)](96)
3188	3077	3093	3100	R3[ν(CH)](98)
3182	3070	3063		R3[ν(CH)](95)
3159	3048	3049		R3[ν(CH)](99)
3094	2986	3010		ν(C17H)(99)
3067	2959	2961	2959	R2[$\nu_a(CH_2)$](100)
3030	2924	2918	2924	R2[$\nu_s(CH_2)$](99)
1874	1808	1827		R2[ν(C16=O)(75)+ν(NC)(10)]
1785	1722	1788	1776	R2[ν(C12=O)(65)+ν(NC)(10)+δ_{in}(NH)(5)]
1720	1660	1688	1686	ν(C34=O)(61)+δ(O25HC34)(7)+R3[ν(C26C34)(5)+ρ(C34C)(5)]+ν(O25C)(5)
1663	1605	1653		R3[$\delta(NH_2)$(64)+ν(N24C)(8)+ν(CC)(15)]
1660	1602	1620		ν(N8C)(53)+R1[ν(C15C17)(15)+ρ(C17H)(15)+ν(CC)(7)]
1647	1590			R3[$\delta(NH_2)$(23)+ν(CC)(48)+δ_{in}(CH)(7)+δ_a(5)]
1627	1570	1603	1612	R3[ν(CC)](64)+δ_{in}(CH)(15)+δ'_a(6)]
1606	1550	1583		R1[ν(CC)(40)+$\nu_a(NO_2)$(27)+$\rho(NO_2)$(6)+δ_{in}(CH)(5)]+ν(N8C)(7)
1585	1530	1562	1566	R1[$\nu_a(NO_2)$(68)+ν(CC)(14)]
1530	1476	1512	1512	R3[δ_{in}(CH)(48)+ν(CC)(34)]
1528	1475	1491	1485	R1[ν(CC)(42)+δ_{ring}(13)+ν(C15C17)(12)+ν(C13N)(5)]+ν(N8C)(5)R2[ν(N7N8)](3)
1497	1445	1464		R3[ν(CC)(37)+δ_{in}(CH)(23)+δ_{in}(C26C34)(6)+ν(N24C)(6)+$\rho(NH_2)$](5)]
1486	1434	1427	1437	R2[$\delta_{sci}(CH_2)$](92)

1446	1396	1400	1399	δ(O25HC34)(46)+ν(O25C)(17)+ν(C34=O)(8)+R3[(δ(C34OO)(8)+ν(C26C34)(6)]
1427	1377	1385	1382	R1[ν(CC)(24)+ν(CO)(26)+δ_{in}(CH)(15)+δ_{in}(C15C17)(5)+ρ(C17H)(5)]
1421	1371			R2[δ_{in}(NH)(58)+ν(C12=O)(9)+ν(NC)(8)]
1398	1349	1367	1372	R2[δ_{in}(NH)(11)+ν(NC)(13)+ν(N7N8)(5)]+R1[ρ(C17H)(9)+ν(CC)(12)+ν(O3N)(7)+ν(N14=O6)(5)]
1388	1339			R2[ν(NC)(32)+ν(CC)(13)+δ_{in}(C12=O)(12)+δ_{ring}(5)]+R1[ρ(C17H)](6)
1364	1317	1352	1344	R1[ν_s(NO_2)(35)+ν(C13N)(16)+ρ(C17H)(14)+δ(NO_2)(11)+ν(CC)(5)]
1362	1314	1319	1321	R3[ν(CC)(79)+δ_{in}(CH)(15)]
1347	1300			R3[δ_{in}(CH)(46)+ν(N24C)(12)+ρ(NH_2)(6)+ν(CC)(10)]
1343	1296	1288	1289	R2[ω(CH_2)(37)+ν(CC)(8)+δ_{ring}(6)+ν(NC)(9)]+R1[ρ(C17H)](15)
1312	1266	1263	1264	R3[ν(N24C)(22)+δ_{in}(CH)(28)+δ_{tring}(11)+ν(C26C34)(7)+ν(CC)(9)]+δ(O25HC34)(9)
1292	1247			R1[ν(CC)(29)+ν(C15C17)(12)+ν(CO)(12)+ν_s(NO_2)(13)+δ_{in}(CH)(7)+ρ(C17H)(7)]
1272	1228	1250	1252	R2[ν(N7N8)(20)+ν(NC)(11)+δ(N8C17N7)(5)]+R1[ν(CO)](15)+ν(O25C)(7)
1271	1226	1238	1239	ν(O25C)(29)+δ(O25HC34)(18)+R3[ν(C26C34)(8)+ν(N24C)(6)+δ(C34OO)(5)]
1249	1205			R1[ν(CO)(31)+δ'_{ring}(9)+ν(C13N)(7)+ν(CC)(5)+R2[ν(N7N8)(18)+ν(NC)(7)]
1211	1168	1219	1220	R2[ν(NC)(52)+ω(CH_2)(22)+δ'_{ring}(5)]
1196	1154	1167	1176	R3[δ_{in}(CH)(72)+ν(CC)(15)]
1195	1154			R1[δ_{in}(CH)(45)+ν(C13N)(9)+δ'_{ring}(7)+ν(CO)(6)+ν(C15C17)(5)]
1189	1148			R2[γ(CH_2)](95)
1145	1104	1117	1117	R3[δ_{in}(CH)(41)+ρ(NH2)(16)+ν(CC)(22)]+ν(O25C)(6)
1131	1091	1109		R2[ν(NC)(49)+δ_{in}(C16=O)(8)+δ_{in}(NH)(6)]
1127	1087	1067		R3[ν(CC)(26)+δ_{in}(CH)(17)+ρ(NH_2)(6)+ν(C26C34)(5)]+R2[ν(NC)](13)+ν(O25C)(9)
1086	1048	1026	1030	R3[ρ(NH_2)(43)+ν(CC)(38)+δ_{in}(CH)(8)]
1041	1004	991	993	R1[δ_{in}(CH)(63)+ν(CC)(25)]
1021	985			R2[ρ(CH_2)(69)+oop(C12=O)(16)+τ(7)]
1016	981			R3[δ_{tring}(63)+ν(CC)(36)]
1001	966	982	984	R1[ν(CO)(53)+δ'_{ring}(14)+ν(C15C17)(8)]
992	957			R3[oop(CH)(87)+puck(9)]
986	951	966	968	R1[δ_{ring}(42)+ν(CO)(18)+ν(CC)(13)+ν(C13N)(8)]
938	906	920	921	R3[ν(CC)(25)+ν(N24C)(14)+ν(C26C34)(12)+δ_a(9)+δ_{in}(C32H)(5)+ν(O25C)(9)
931	898	912	912	R1[ω(C17H)(54)+oop(CH)(10)]+τ(N8C17)(23)
927	895	885	887	R3[oop(CH)(71)+puck(9)+oop(C26C34)(8)+τ_a(6)]
919	887			R2[ν(CC)(58)+ν(NC)(13)+δ_{in}(C12=O)(6)+δ_{in}(C16=O)(5)]
911	879	876		R1[oop(CH)(76)+τ(13)]
907	876			R3[oop(CH)(43)+puck(7)+oop(C37N)(6)]+τ(O25H40)(14)+τ(O25C)(14)+R2[oop(NH)](6)
905	874			R3[oop(CH)(46)+oop(C37N)(6)+puck(6)]+τ(O25H40)(13)+τ(O25C)(12)+R2[oop(NH)](6)
880	849	854		R1[δ'_{ring}(18)+δ(C15C17N)(14)]+R2[δ(N8C17N7)(16)+ν(NC)(19)+δ'_{ring}(8)+ν(N7N8)(7)]
873	843	835		R2[oop(NH)](36)+τ(O27H)(26)+τ(O25H40)(18)+τ(O25C)(16)
830	801	810	812	R1[δ_{sci}(NO_2)(59)+δ'_{ring}(17)+δ_{ring}(7)+ν(O3N)(5)
824	795			R3[oop(CH)(49)+ω(C34C)(19)+puck(16)+oop(C26C34)(12)]
823	795	787		R1[oop(CH)(82)+τ'(6)]
788	760	762	790	R2[ν(NC)(23)+δ'_{ring}(7)+δ_{in}(C16=O)(6)+R1[δ'_{ring}(13)+δ_{ring}(11)+ν(C15C17)(6)+δ(NOO-)(5)]
772	745	752	754	R3[ω(C34C)(27)+oop(CH)(32)+oop(C37N)(9)+δ(C34OO)(6)]
767	740			R3[(δ(C34OO)(22)+ω(C34C)(8)+δ'a(7)+δ_{tring}(7)+ν(C26C34)(6)+oop(CH)(6)+ν(CC)(7)]+δ(O1O25C34)(7)+ν(O25C)(5)
767	740	737	736	R1[ω(N14C)(69)+oop(C13N)(15)+τ'(8)+oop(CH)(5)]
754	727			R2[oop(C16=O)(69)+τ'(14)+τ(9)]
699	674	687	696	R3[puck(67)+oop(C37N)(14)+oop(CH)(12)+oop(C26C34)(5)]
698	673		664	R1[τ'(36)+oop(C15C17)(34)+τ(24)]
691	667			R2[δ_{ring}(28)+ν(NC)(14)+δ'_{ring}(12)+δ_{in}(C16=O)(10)+δ_{in}(N7N)(8)+δ_{in}(C12=O)(5)+ν(CC)(5)]
673	650	656	655	R3[(δ(C34OO)(36)+δ_a(31)+δ'_a(13)]+δ(O1O25C34)(7)
631	609	625	629	R2[δ_{in}(C12=O)(23)+δ_{in}(C16=O)(16)+δ_{ring}(13)+δ_{in}(N7N)(10)+δ'_{ring}(9)+δ(N8C17N7)(6)]
610	589	609	608	R2[δ'_{ring}(31)+δ_{ring}(14)+ν(NC)(17)+ν(C12=O)(5)]
602	581			R1[τ(51)+τ'(25)+oop(C13N)(17)]
596	575		579	R2[oop(C12=O)(57)+ρ(CH_2)(15)+τ(15)+γ(CH_2)(7)]
583	562	573	570	R3[ω(N24C)(41)+oop(C37N)(16)+ν(N24C)(6)+τ'_a(6)+τ_a(5)+oop(C26C34)(5)+puck(5)]
564	544	550	550	R3[δ'_a(30)+ρ(C34C)(29)+δ_{in}(C26C34)(6)+δ_a(6)]
554	534			R1[ρ(NO_2)(43)+δ_{in}(C13N)(21)+δ_{in}(C15C17)(10)+ν(CC)(5)]+R2[δ(N8C17N7)](5)
534	515	511	514	R3[ω(N24C)(27)+oop(C37N)(19)+τ_a(14)+τ'_a(11)+oop(C26C34)(9)]
516	498	471	471	R3[δ'_a(17)+ρ(C34C)(16)+ν(N24C)(12)+ω(N24C)(12)+δ_{in}(C26C34)(11)+δ_{in}(C37N)(7)]
465	449	447	447	R2[δ(N8C17N7)(17)+δ_{in}(C12=O)(8)+δ_{in}(N7N)(5)]+R1[ν(C13N)(13)+δ_{in}(C15C17)(11)+ρ(NOO)(11)+δ_{ring}(5)+δ(NOO-)(5)]
451	435		431	R2[δ_{in}(C16=O)(14)+δ_{in}(C12=O)(14)+ν(NC)(6)+R1[δ_{in}(C15C17)(10)+δ(C15C17N)(7)+ν(C13N)(6)+ρ(

				NOO)(5)]
442	426		425	R3[τ_a(36)+τ'_a(32)+oop(C26C34)(14)+oop(CH)(9)]
417	403	422		R1[ν(C13N)(20)+δ(NOO-)(7)+δ_{ring}(6)]+R2[δ_{in}(C12=O)(12)+δ_{in}(C16=O)(5)]+R3[δ_{in}(C37N)(8)+δ_a(5)]
413	399		407	R3[δ_a(28)+δ_{in}(C37N)(17)+ν(C26C34)(13)+δ(C34OO)(6)]+ν(O1H40)(5)
386	372	-	38	τ(N8C17)(27)+R1[τ'(16)+τ(14)+oop(C15C17)(9)+ω(C17H)(8)+oop(C13N)(7)+R2[oop(N7N)](8)
374	361	-		R3[δ_{in}(C37N)(40)+ρ(C34C)(16)+ν(C26C34)(9)+ν(CC)(6)]+ν(O1H40)(9)
312	301	-	302	R3[τ(N24C)](92)
309	298	-		R2[τ(N7N)(39)+oop(N7N)(23)+τ'(10)]+R1[τ(C15C17)](12)+τ(N8C17)(6)
293	283	-	260	R2[δ_{in}(N7N)(18)+δ_{in}(C16=O)(16)+ν(NC)(7)+δ(N8C17N7)(5)]+R1[δ_{in}(C13N)(13)+δ_{in}(C15C17)(11)+ρ(NOO)(7)+ν(C15C17)(6)]
232	224	-	235	R3[δ_{in}(C26C34)(32)+δ_{in}(C37N)(9)]+δ(O1O25C34)(23)+ν(O27H23)(7)
228	220	-	231	R1[δ_{in}(C13N)(21)+ρ(NOO)(12)+δ(C15C17N)(8)+ν(C15C17)(5)]+ν(O1H40)(10)+R3[δ_{in}(C26C34)](6)
228	220	-	202	R3[τ'_a(41)+τ_a(23)+puck(11)+oop(CH)(12)]
200	193	-	187	R1[oop(C13N)(49)+oop(C15C17)(7)+R2[τ(N7N)(13)+oop(NH)(5)]+τ(N8C17)(6)
190	183	-	179	R2[τ'(71)+oop(N7N)(16)]
172	166	-		R2[τ(20)+oop(NH)(9)+τ'(5)]+R3[oop(C26C34)(17)+τ_a(12)+oop(C28H)(7)]+τ(O1O25)(8)+τ(O25C)(8)
166	160	-		R2[τ(48)+oop(NH)(33)]
163	157	-	142	ν(O1H40)(27)+δ(O1O25C34)(18)+R2[δ_{in}(N7N)(13)+δ(N8C17N7)(10)]+R1[δ_{in}(C13N)](13)
133	128	-	108	R1[oop(C13N)(20)+oop(C15C17)(13)+τ(C13N)(12)]+R2[τ(8)+τ(C15C17)(5)+oop(N7N)(18)]
91	88	-	-	R1[τ(C13N)(29)+τ(C15C17)(6)]+R2[oop(N7N)(22)+oop(NH)(10)+τ'(8)]+τ(O27H)(9)
90	87	-	-	δ(O1O25C34)(46)+ν(O1H40)(12)+R1[δ_{in}(C15C17)(9)+δ(C15C17N)(5)]+δ(O25HC34)(5)
84	81	-	-	ν(O27H23)(39)+ν(O1H40)(23)+δ(O25HC34)(10)+δ(O1O25C34)(6)
73	70	-	-	τ(O1O25)(38)+R3[τ(C26C34)](27)+τ(O25C)(12)+τ(O27H)(9)+τ(O25H40)(8)
62	60	-	-	R1[τ(C13N)(35)+oop(C15C17)(8)]+R2[oop(NH)](15)+τ(O25C)(10)+τ(O27H)(9)
59	57	-	-	ν(O27H23)(17)+R1[(δ(C15C17N)(14)+δ_{in}(C15C17)(14)]+ν(O1H40)(11)+R3[ρ(C34C)(10)+δ_{in}(C26C34)(7)]+δ(O1O25C34)(9)+R2[δ(N8C17N7)](5)
43	41	-	-	R1[τ(C15C17)(25)+τ(C13N)(14)]+τ(O25C)(12)+R2[oop(N7N)(10)+τ(N7N)(7)]+R3[τ(C26C34)](6)
29	28	-	-	τ(O1O25)(25)+R2[oop(N7N)](17)+τ(O25H40)(17)+τ(O27H)(10)+R3[τ(C26C34)](9)+τ(N8C17)(5)
25	24	-	-	ν(O27H23)(23)+R1[(δ(C15C17N)(17)+δ_{in}(C15C17)(10)]+R2[δ(N8C17N7)](14)+ν(O1H40)(10)+R2[δ_{in}(N7N)](8)
22	21	-	-	R1[τ(C15C17)](17)+τ(O1O25)(15)+τ(O27H)(15)+R2[τ(N7N)(12)+oop(NH)(5)]+τ(O25C)(10)+R3[τ(C26C34)](9)
12	12	-	-	τ(O25H40)(37)+τ(O1O25)(25)+R2[oop(N7N)(16)+oop(NH)(10)]

Table S4 Theoretical and experimental vibrational wavenumbers (in cm^{-1}) of NF and their assignments.

Scaled DFT				Potential Energy Distribution (≥5%)
B3LYP/cc-pvTZ	**wB97X-D/cc-pvTZ**	**Raman**	**IR**	
3503	3516	-	3287	R2[ν(NH)](100)
3168	3156	-	3148	R1[ν(CH)](96)
3137	3122	-	3109	R1[ν(CH)](99)
2987	2993	-	3017	ν(C13H)(99)
2964	2965	-	2948	R2[$\nu_a(CH_2)$](100)
2927	2915	-	2916	R2[$\nu_s(CH_2)$](99)
1809	1836	1980	1782	R2[ν(C10=O)(63)+ν(C11=O)(16)+δ'_{ring}(6)+ν(NC)(5)]
1771	1798		1744	R2[ν(C11=O)(63)+ν(C10=O)(16)+ν(NC)(6)]
1603	1648	1608	1651	ν(C13=N)(54)+R1[ρ(C13H)(15)+ν(C13C14)(15)+ν(CC)(6)]
1551	1601	1563	1605	R1[ν(CC)(39)+ν(N9=O4)(15)+ν(NO)(12)+ρ(NOO)(6)+δ_{in}(CH)(8)]+ν(C13=N)(7)
1531	1570		1566	R1[ν(N9=O4)(38)+ν(NO)(30)+ν(CC)(14)]+ν(C13=N)(5)
1475	1500	1509	1520	R1[ν(CC)(42)+δ_{ring}(13)+ν(C13C14)(12)+ν(NC)(5)]+ν(C13=N)(5)
1436	1413	1492	1489	R2[δ(CH2)](91)
1377	1401	1428	1427	R1[ν(CC)(17)+ν(OC)(28)+δ_{in}(CH)(15)+ν(CC)(7)+δ_{in}(C13C14)(5)+ρ(C13H)(5)
1356	1374	1378	1381	R2[ν(NC)(12)+ω(CH2)(9)+ν(NN)(6)]+R1[ρ(C13H)(11)+ν(CC)(14)+δ_{in}(CH)(5)]
1326	1357			R2[δ_{in}(NH)(28)+ν(NC)(16)+$\omega(CH_2)$(5]+R1[ν(NO)(8)+ν(N9=O4)(6)+ρ(C13H)(5)+ν(NC)(5)]
1318	1336	1348	1350	R1[ρ(C13H)(23)+ν(NO)(17)+ν(NC)(13)+ν(N9=O4)(11)+δ(NOO)(9)+ν(CC)(9)]
1300	1310	1323	1342	R2[δ_{in}(NH)(28)+$\omega(CH_2)$(17)+ν(NC)(24)]
1279	1291			R2[ν(CC)(19)+$\omega(CH_2)$(19)+ν(NC)(25)+δ_{in}(C11=O)(10)+δ_{ring}(6)]+R1[ρ(C13H)](6)
1246	1262	1258		R1[ν(CC)(28)+ν(C13C14)(12)+ν(OC)(11)+ν(NO)(7)+δ_{in}(CH)(7)+ρ(C13H)(6)+ν(N9=O4)(6)]

1225	1252	1247	1250	R2[ν(NN)(20)+ν(NC)(11)+δ(N8C13N7)(5)]+R1[ν(OC)(25)+δ'_{ring}(6)+δ_{in}(CH)(10)]
1204	1235	1235	1242	R2[ν(NN)(23)+ν(NC)(8)]+R1[ν(OC)(28)+δ'_{ring}(8)+ν(NC)(6)]
1168	1188	1207	1211	R2[ω(CH_2)(23)+ν(NC)(49)]
1153	1147			R1[δ_{in}(CH)](49)+ν(NC)(10)+δ'_{ring}(8)+ν(OC)(7)+ν(C13C14)(5)]
1151	1132	1169		R2[γ(CH_2)](96)
1077	1094	1121	1111	R2[ν(NC)(60)+δ_{in}(C10=O)(10)+δ_{in}(NH)(10)+ν(CC)(5)]
1004	991	1017	1018	R1[δ_{in}(CH)(63)+ν(CC)(25)]
983	979			R2[ρ(CH_2)(70)+oop(C11=O)(15)+τ(7)]
966	968	977		R1[ν(OC)(52)+δ'_{ring}(14)+ν(C13C14)(8)]
951	957	962	964	R1[δ_{ring}(42)+ν(OC)(18)+ν(CC)(13)+ν(NC)(8)]
898	894	902	926	R1[ω(C13H)(56)+oop(CH)(9)+τ(N8C13)(24)
878	873		903	R1[oop(CH)(77)+τ(13)]
860	863		872	R2[ν(CC)(54)+ν(NC)(18)+δ_{in}(NH)(7)]
849	854	869		R1[δ'_{ring}(17)+δ(C13C14N)(15)+R2[δ(N8C13N7)(17)+ν(NC)(13)+δ'_{ring}(8)+ν(NN)(8)+ν(NC)(6)]
801	810	809	833	R1[δ(NOO)(59)+δ'_{ring}(17)+δring(7)+ν(NO)(5)]
793	791		826	R1[oop(CH)(83)+τ'(6)]
760	764	783	779	R2[ν(NC)(21)+δ'_{ring}(8)+δ_{in}(C10=O)(5)+R1[δ'_{ring}(15)+δ_{ring}(12)+ν(C13C14)(7)+δ(NOO)(5)]
739	746		725	R1[ω(N9C)(68)+oop(C15N)(14)+τ'(8)+oop(CH)(5)]
725	734		725	R2[oop(C10=O)(70)+τ'(14)+τ(9)]
673	676	685		R1[τ'(36)+oop(C13C14)(34)+τ(24)]
667	670		687	R2[δ_{ring}(26)+ν(NC)(16)+δ'_{ring}(11)+δ_{in}(C10=O)(10)+δ_{in}(N7N)(10)+δ_{in}(C11=O)(5)+ν(CC)(5)]
603	594		606	R2[oop(NH)(45)+oop(C11=O)(35)+τ(11)+ρ(CH_2)(6)]
595	591	622		R2[δ_{in}(C11=O)(18)+δ'_{ring}(16)+δ_{in}(C10=O)(14)+δ_{ring}(10)+δ_{in}(N7N)(10)+δ(N8C13N7)(6)+ν(NC)(7)]
582	584			R2[δ'_{ring}(23)+δ_{ring}(20)+ν(NC)(14)]+R1[ν(C13C14)](5)
581	583	606	571	R1[τ(52)+τ'(25)+oop(C15N)(17)]
542	534		548	R2[oop(NH)(43)+oop(C11=O)(33)+ρ(CH_2)(12)+γ(CH_2)(6)+τ(5)]
533	529	551		R1[ρ(NOO)(43)+δ_{in}(C15N)(21)+δ_{in}(C13C14)(10)+ν(CC)(5)]
447	450	468	463	R2[δ(N8C13N7)(17)+δ_{in}(C10=O)(5)+δ_{in}(N7N)(5)]+R1[δ_{in}(C13C14)(14)+ρ(NOO)(12)+ν(NC)(11)+δ_{ring}(6)+δ(C13C14N)(5)]
426	430	438	440	R1[ν(NC)(19)+δ(NOO)(8)+δin(C13C14)(6)+δ(C13C14N)(6)+δ'_{ring}(5)]+R2[δ_{in}(C11=O)(12)+δ_{in}(C10=O)(7)+ν(NC)(5)+δ_{ring}(5)]
386	388	386	409	R2[δ_{in}(C11=O)(33)+δ_{in}(C10=O)(10)+ν(NC)(6)+ν(CC)(6)+ν(NC)(9)]+R1[ν(NC)(11)+δ_{ring}(6)]
373	373	381		τ(N8C13)(28)+R1[τ'(16)+τ(14)+oop(C13C14)(9)+ω(C13H)(8)+oop(C15N)(8)]+R2[oop(N7N)](8)
297	284			R2[τ(NN)(39)+τ(C13C14)(11)+oop(N7N)(23)+τ'(10)]+τ(N8C13)(6)
283	279	295	-	R2[δ_{in}(N7N)(18)+δ_{in}(C10=O)(17)+ν(NC)(6)]+R1[δ_{in}(C15N)(13)+δ_{in}(C13C14)(12)+ρ(NOO)(7)+ν(C13C14)(6)]
214	217	216	-	R1[δ_{in}(C15N)(33)+ρ(NOO)(18)+δ(C13C14N)(12)+ν(C13C14)(6)+δ_{ring}(5)]
193	189	204	-	R1[oop(C15N)(50)+oop(C13C14)(7)]+τ(N8C13)(6)+R2[τ(NN)(14)+oop(N7N)(5)]
181	165	-	-	R2[τ'(76)+oop(N7N)(17)]
144	138	-	-	R2[τ(54)+oop(NH)(36)]
131	135	-	-	R2[δ_{in}(N7N)(30)+δ(N8C13N7)(20)]+R1[δ_{in}(C15N)(17)+δ_{in}(C13C14)(13)]
122	116	-	-	R2[τ(32)+oop(NH)(18)+oop(N7N)(5)]+R1[oop(C15N)(12)+oop(C13C14)(10)+τ(C15N)(10)]
77	70	-	-	R1[τ(C15N)(46)+τ(C13C14)(5)+R2[oop(N7N)(31)+τ'(5)+τ(NN)(5)]
49	50	-	-	R1[(δ(C13C14N)(35)+δ_{in}(C13C14)(29)+δ_{in}(C15N)(5)]+R2[δ(N8C13N7)(18)+δ_{in}(N7N)(6)]
44	36	-	-	R1[τ(C15N)(27)+τ(C13C14)(15)+oop(C13C14)(11)]+R2[oop(N7N)(24)+τ'(5)]
25	22	-	-	R1[τ(C13C14)](29)+R2[oop(N7N)(25)+τ(NN)(20)+τ(N8C13)(11)

Table S5 Theoretical and experimental vibrational wavenumbers (in cm^{-1}) of 3-ABA and their assignments.

Scaled DFT		Raman	IR	Potential Energy Distribution (≥5%)
B3LYP/cc-pvTZ	WB97XD/cc-pvTZ			
3626	3670		3559	R[ν(OH)](100)
3537	3548		3432	R[ν_a(NH_2)(99)
3441	3449		3300	R[ν_s(NH_2)(99)

3109	3110		3146	R[ν(CH)](96)
3074	3068		3076	R[ν(CH)](97)
3069	3065		3067	R[ν(CH)](98)
3049	3045		3044	R[ν(CH)](99)
1725	1757	1696	1751	R[ν(C4=O)(77)+ν(C4C5)(10)]
1605	1617	1614	1638	R[ν(CC)(55)+δ(NH_2)(9)+δ_a(8)+ν(NC)(7)+δ_{in}(CH)(14)]
1590	1594	1611		R[δ(NH_2)(27)+ν(CC)(47)+δ'_a(7)+δ_{in}(CH)(7)]
1571	1588	1609	1568	R[δ(NH_2)(52)+ν(CC)(31)]
1476	1480	1514	1524	R[δ_{in}(CH)(45)+ν(CC)(39)]
1444	1450	1482	1450	R[ν(CC)(38)+δ_{in}(CH)(23)+ν(NC)(8)+δ_{in}(C4C5)(6)]
1327	1341	1381	1387	R[ν(O3C)(22)+ν(C4C5)(20)+δ(O3HC)(19)+δ(C4OO)(13)]
1313	1302	1351		R[ν(CC)(73)+δ_{in}(CH)(24)]
1297	1291	1327	1310	R[δ_{in}(CH)(41)+ν(NC)(12)+ν(CC)(23)+ρ(NH_2)(9)
1254	1256	1286	1292	R[ν(NC)(26)+δ_{in}(CH)(31)+δ_{tring}(9)+ν(CC)(10)+δ(O3HC)(5)]
1159	1161	1224	1221	R[δ(O3HC)(33)+δ_{in}(CH)(26)+ν(O3C)(15)+ν(C4C5)(8)+ν(CC)(9)]
1138	1146	1173	1165	R[δ(O3HC)(20)+δ_{in}(CH)(46)+ν(O3C)(12)+ν(CC)(9)]
1100	1098	1144	1138	R[δ_{in}(CH)(43)+ρ(NH2)(17)+ν(CC)(19)+ν(O3C)(7)]
1077	1082	1093	1094	R[ν(CC)(31)+δ_{in}(CH)(30)+ν(O3C)(14)+ν(C4C5)(6)]
1044	1047	1040	1070	R[ρ(NH_2)(47)+ν(CC)(35)+δ_{in}(CH)(5)]
981	979	1005	1003	R[δ_{tring}(64)+ν(CC)(34)]
956	959	993	980	R[oop(CH)(85)+puck(10)]
897	902			R[ν(CC)(25)+ν(NC)(15)+ν(C4C5)(11)+ν(O3C)(10)+δa(9)+oop(CH)(5)+δ_{in}(CH)(5)]
893	895	912	918	R[oop(CH)(72)+oop(C4C5)(8)+τ'_a(6)+puck(6)]
874	876	861	895	R[oop(CH)(67)+puck(15)+oop(CN)(10)]
795	794	824	822	R[ω(C4C)(24)+oop(CH)(47)+puck(13)+oop(C4C5)(12)]
745	748	797	789	R[ω(C4C)(27)+oop(CH)(42)+oop(CN)(13)+puck(7)]
719	720	726	756	R[δ'_a(21)+δ(C4OO)(16)+ν(C4C5)(12)+δ_{tring}(11)+ν(CC)(12)+ν(O3C)(5)+ν(NC)(5)]
678	677	667		R[puck(67)+oop(CH)(13)+oop(CN)(10)+oop(C4C5)(6)]
622	623	640	675	R[(δ(C4OO)(49)+δ'_a(34)+δ(O3HC)(7)]
599	599	623	669	R[τ(O3C)(45)+oop(CN)(21)+τ_a(10)+oop(C4C5)(8)+ω(NC)(8)]
554	552	551	550	R[ω(NC)(53)+τ(O3C)(12)+δ_a(10)+ν(NC)(6)+puck(5)]
536	535	549	527	R[δ_a(39)+ρ(C4C)(19)+ν(NC)(17)]
501	498	519	509	R[τa(26)+oop(CN)(23)+ω(NC)(15)+τ(O3C)(9)+oop(C4C5)(6)+ω(C4C)(5)]
488	489	504		R[ρ(C4C)(23)+δ_{in}(C4C5)(18)+CN)(13)+δ_a(12)+ν(NC)(13)]
422	417	443	451	R[τ'_a(68)+oop(C4C5)(14)+oop(CH)(5)]
385	385	410		R[δ_{in}(CN)(31)+δ'_a(26)+ν(C4C5)(13)+ρ(C4C)(7)+δ(C4OO)(6)+δ_a(5)]
342	344	347	-	R[δ_{in}(CN)(35)+ρ(C4C)(19)+ν(C4C5)(12)+δ(C4OO)(11)+ν(CC)(8)]
304	297	321	-	R[τ(NC)](92)
219	219	-	-	R[τ_a(65)+puck(12)+oop(CH)(12)]
183	183	-	-	R[δ_{in}(C4C5)(62)+ρ(C4C)(17)+δ_{in}(CN)(10)]
150	146	-	-	R[oop(C4C5)(42)+τ'_a(19)+oop(CH)(11)+ω(C4C)(9)+oop(CH)(6)]
58	54	-	-	R[τ(C4C5)(87)+τ_a(7)]

Table S6 (a) Calculated and observed ^{13}C NMR chemical shifts (δ/ppm) of NF-3ABA, NF and 3ABA using wB97X-D/cc-pvTZ.

Atom	δ_{cal}	δ_{exp}	Atom	δ_{cal}	δ_{exp}
NF-3ABA			**NF**		
C12	178.121	174.602	C11	168.796	168.9
C34	177.645	171.077	C15	159.744	151.9
C13	159.313	150.811	C14	155.744	151.9
C15	155.024	150.811	C10	153.666	151.9
C16	153.961	150.811	C13	129.32	133.1
C37	153.779	149.40	C17	117.869	118.2
C26	136.634	131.523	C16	116.652	118.2
C32	135.009	131.523	C12	48.1919	49.8
C17	128.662	131.523	**3ABA**		
C35	125.2	118.453	C4	171.356	172.399
C30	122.942	118.453	C7	154.204	136.859
C28	120.989	118.453	C 5	135.832	130.006
C21	117.762	115.075	C 9	135.066	126.873
C19	117.568	115.075	C10	124.881	126.873
C9	48.1229	47.950	C8	122.8	126.873
			C6	121.122	123.250

Table S6 (b) Calculated and observed ^{13}C NMR chemical shifts (δ/ppm) of NF-3ABA, NF and 3ABA using B3LYP/cc-pvTZ.

Atom	δ_{cal}	δ_{exp}	Atom	δ_{cal}	δ_{exp}
	NF-3ABA			**NF**	
C34	178.37	174.602	C11	168.49	168.9
C12	177.921	171.077	C15	161.802	151.9
C13	161.601	150.811	C14	158.587	151.9
C15	158.621	150.811	C10	153.998	151.9
C37	154.304	150.811	C13	127.858	133.1
C16	154.179	149.40	C17	118.91	118.2
C26	136.49	131.523	C16	117.3	118.2
C32	133.945	131.523	C12	50.1449	49.8
C17	127.453	131.523		**3ABA**	
C35	124.825	118.453	C4	172.199	172.399
C30	123.009	118.453	C7	154.369	136.859
C28	120.64	118.453	C 5	135.603	130.006
C19	118.501	115.075	C 9	134.27	126.873
C21	117.492	115.075	C10	124.74	126.873
C9	49.7997	47.950	C8	122.536	126.873
			C6	120.709	123.250

Table S7 Results of correlation analysis for ^{13}C shifts (in ppm) with GIAO scheme.

Molecule	Functional	b	a	S_0	R^2	mae
NF-3ABA	B3LYP	0.95785±0.02	1.81088±3.25	2.76962	0.99616	4.46
	wB97X-D	0.96124±0.02	1.76111±2.62	2.23697	0.9975	3.87
NF	B3LYP	0.95248±0.04	4.63059±6.24	4.66822	0.99322	3.29
	wB97X-D	0.95091±0.03	5.68234±4.47	3.38138	0.99645	2.60

'a' is the intercept and b is the slope of the correlation line, 'R^2' is the square of correlation coefficient, 'S_0' is the standard deviation of the points from the correlation line, and 'mae' is the mean absolute error.

Table S8 Selected second order perturbation theory analysis of Fock matrix in NBO Basis of NF-3ABA using wB97X-D/cc-pvTZ level of theory.

Donor NBO (i)	ED(i)/e	Acceptor NBO (j)	ED(j)/e	E(2)[a] kcal/mol	E(j)-E(i)[b] a.u.	F(i,j)[c] a.u.
			within unit 1			
πO6-N14	1.98470	n(3)O3	1.46697	10.34	0.23	0.083
		π*O6-N14	0.61685	6.13	0.45	0.056
πN8-C17	1.93121	π*C15-C19	0.30698	14.27	0.49	0.079
σC9-C12	1.97456	σ*N7-N8	0.02646	6.66	1.22	0.081
πC13-C21	1.80341	π*O6-N14	0.61685	27.00	0.28	0.087
		π*C15-C19	0.30698	23.15	0.43	0.091
σC15-C17	1.97694	σ*N7-N8	0.02646	6.14	1.27	0.079
πC15-C19	1.78384	π*N8-C17	0.21481	21.73	0.41	0.084
		π*C13-C21	0.29892	29.72	0.41	0.101
σC17-H18	1.98049	σ*O2-C15	0.02623	6.37	1.09	0.074
σC19-C21	1.96940	σ*C13-N14	0.11984	9.46	1.14	0.095
		σ*C15-C17	0.03086	7.07	1.30	0.085
n(1)O1	1.96518	σ*N5-C12	0.06726	6.63	1.33	0.085
n(2)O1	1.85055	σ*N5-C12	0.06726	24.55	0.90	0.136
		σ*C9-C12	0.07044	30.43	0.78	0.141
n(2)O2	1.69598	π*C13-C21	0.29892	45.29	0.47	0.131
		π*C15-C19	0.30698	46.48	0.48	0.133
n(2)O3	1.89149	σ*O6-N14	0.05653	24.54	0.89	0.134
		σ*C13-N14	0.11984	19.12	0.72	0.105
n(3)O3	1.46697	π*O6-N14	0.61685	239.34	0.22	0.209
n(2)O4	1.82258	σ*N5-C16	0.09367	38.50	0.78	0.158
		σ*N7-C16	0.11084	40.99	0.77	0.162
n(1)N5	1.62062	π*O1-C12	0.28629	101.02	0.37	0.177
		π*O4-C16	0.28510	61.26	0.40	0.142

n(2)O6	1.88777	σ*O3-N14	0.05834	25.25	0.88	0.135
		σ*C13-N14	0.11984	22.25	0.72	0.113
n(1)N7	1.66646	π*O4-C16	0.28510	66.38	0.41	0.149
		π*N8-C17	0.21481	50.44	0.40	0.131
		σ*C9-H10	0.02096	7.36	0.76	0.073
		σ*C9-H11	0.02101	7.42	0.76	0.073
n(1)N8	1.90986	σ*N7-C9	0.04285	16.91	0.85	0.108
		σ*C17-H18	0.03332	13.13	0.91	0.099
π*O6-N14	0.61685	π*C13-C21	0.29892	22.41	0.14	0.075
			from unit 1 to unit 2			
n(1)O1	1.96518	σ*O25-H40	0.05126	6.53	1.31	0.083
n(2)O1	1.85055	σ*O25-H40	0.05126	17.88	0.88	0.115
			from unit 2 to unit 1			
n(1)O27	1.96208	σ*N5-H23	0.04640	8.88	1.29	0.096
n(2)O27	1.86532	σ*N5-H23	0.04640	12.04	0.86	0.093
			within unit 2			
σO25-H40	1.98560	σ*C26-C34	0.06809	6.03	1.34	0.081
πC26-C35	1.65981	π*O27-C34	0.27488	28.52	0.36	0.092
		π*C28-C37	0.36933	29.45	0.39	0.096
		π*C30-C32	0.33730	36.52	0.39	0.106
σC28-H29	1.97408	σ*C26-C35	0.02106	6.03	1.23	0.077
πC28-C37	1.61186	π*C26-C35	0.39790	41.58	0.38	0.113
		π*C30-C32	0.33730	32.04	0.39	0.101
πC30-C32	1.69067	π*C26-C35	0.39790	31.34	0.39	0.101
		π*C28-C37	0.36933	33.12	0.39	0.103
n(1)N24	1.85557	π*C28-C37	0.36933	36.52	0.45	0.122
n(1)O25	1.97230	σ*O27-C34	0.02314	11.02	1.36	0.109
n(2)O25	1.79319	π*O27-C34	0.27488	79.36	0.46	0.173
n(2)O27	1.86532	σ*O25-C34	0.07387	30.28	0.86	0.146
		σ*C26-C34	0.06809	24.55	0.86	0.132
π*O27-C34	0.27488	π*C26-C35	0.39790	114.65	0.03	0.084

Table S9 Second order perturbation theory analysis of Fock matrix in NBO Basis of NF – 3-ABA acid using B3LYP/cc-pvTZ level of theory.

Donor NBO (i)	ED(i)/e	Acceptor NBO (j)	ED(j)/e	E (2)[a] K cal/mol	E(j)-E(i)[b] a.u.	F(i,j)[c] a.u.
			within unit 1			
πO6-N14	1.98241	n(3)O3	1.47097	11.31	0.18	0.077
		π*O6-N14	0.64423	7.58	0.32	0.053
		π*C13-C21	0.31275	5.49	0.44	0.048
πN8-C17	1.91415	π*C15-C19	0.32755	11.77	0.35	0.061
σC9-C12	1.97380	σ*N7-N8	0.02699	5.71	1.04	0.069
πC13-C21	1.77682	π*O6-N14	0.64423	23.01	0.18	0.064
		π*C15-C19	0.32755	14.72	0.30	0.061
σC15-C17	1.97658	σ*N7-N8	0.02699	5.22	1.10	0.068
πC15-C19	1.75257	π*N8-C17	0.24757	18.25	0.28	0.063
		π*C13-C21	0.31275	18.74	0.29	0.066
σC17-H18	1.97906	σ*O2-C15	0.02809	5.91	0.90	0.065
σC19-C21	1.96995	σ*C13-N14	0.11845	8.12	0.98	0.081
		σ*C15-C17	0.02945	6.22	1.13	0.075
n(1)O1	1.96466	σ*N5-C12	0.06843	5.56	1.15	0.072
n(2)O1	1.84785	σ*N5-C12	0.06843	19.51	0.74	0.110
		σ*C9-C12	0.07200	24.45	0.62	0.112
n(2)O2	1.69723	π*C13-C21	0.31275	29.53	0.35	0.091
		π*C15-C19	0.32755	30.35	0.35	0.093
n(2)O3	1.88959	σ*O6-N14	0.05794	18.98	0.71	0.105
		σ*C13-N14	0.11845	14.76	0.57	0.082
n(3)O3	1.47097	π*O6-N14	0.64423	157.41	0.14	0.138
n(2)O4	1.81859	σ*N5-C16	0.09490	29.82	0.62	0.124
		σ*N7-C16	0.11407	32.40	0.61	0.128
n(1)N5	1.60670	π*O1-C12	0.29579	73.47	0.26	0.125
		π*O4-C16	0.29807	48.98	0.28	0.107
n(2)O6	1.88646	σ*O3-N14	0.05999	19.55	0.70	0.106
		σ*C13-N14	0.11845	17.04	0.56	0.088

n(1)N7	1.64349	π*O4-C16	0.29807	49.59	0.29	0.109
		π*N8-C17	0.24757	38.66	0.27	0.095
		σ*C9-H10	0.02143	5.82	0.62	0.059
		σ*C9-H11	0.02143	5.83	0.62	0.059
n(1)N8	1.90422	σ*N7-C9	0.04745	14.42	0.68	0.089
		σ*C17-H18	0.03522	10.49	0.75	0.080
π*O6-N14	0.64423	π*C13-C21	0.31275	21.52	0.12	0.065
π*N8-C17	0.24757	π*C15-C19	0.32755	142.31	0.01	0.071
			from unit 1 to unit 2			
n(1)O1	1.96466	σ*O25-H40	0.05142	5.18	1.13	0.069
n(2)O1	1.84785	σ*O25-H40	0.05142	14.19	0.72	0.092
			from unit 2 to unit 1			
n(1)O27	1.96133	σ*N5-H23	0.04712	7.17	1.12	0.080
n(2)O27	1.86241	σ*N5-H23	0.04712	9.58	0.70	0.075
			within unit 2			
σO25-H40	1.98555	σ*C26-C34	0.06766	5.10	1.16	0.070
πC26-C35	1.65131	π*O27-C34	0.28987	24.79	0.24	0.070
		π*C28-C37	0.37247	18.70	0.28	0.065
		π*C30-C32	0.33688	21.28	0.28	0.069
σC28-H29	1.97591	σ*C26-C35	0.02124	5.05	1.06	0.065
πC28-C37	1.61358	π*C26-C35	0.40188	22.86	0.28	0.072
		π*C30-C32	0.33688	18.00	0.28	0.064
πC30-C32	1.69000	π*C26-C35	0.40188	18.35	0.28	0.066
		π*C28-C37	0.37247	20.81	0.28	0.069
σC35-H36	1.97472	σ*C26-C28	0.01796	5.26	1.05	0.067
n(1)N24	1.84469	π*C28-C37	0.37247	27.12	0.33	0.089
n(1)O25	1.97212	σ*O27-C34	0.02330	9.08	1.17	0.092
n(2)O25	1.79134	π*O27-C34	0.28987	56.27	0.32	0.122
n(2)O27	1.86241	σ*O25-C34	0.07677	24.20	0.68	0.116
		σ*C26-C34	0.06766	19.76	0.70	0.107
π*O27-C34	0.28987	π*C26-C35	0.40188	62.81	0.04	0.075

[a]E(2) means energy of hyper conjugative interaction (stabilization energy), [b]Energy difference between donor (i) and acceptor (j) NBO orbitals, [c]F(i,j) is the Fock matrix element between i and j NBO orbitals.

Table S10 Selected reactivity descriptors as Fukui functions (f_k^+, f_k^-), local softnesses (s_k^+, s_k^-), local electrophilicity indices (ω_k^+, ω_k^-) for NF – 3-ABA acid using wB97X-D/cc-pvTZ.

Sites	f_k^+ (e)	ω_k^+(ev).	s_k^+ (ev^{-1})	f_k^-(e)	ω_k^- (ev).	s_k^- (ev^{-1})	f_k^+/f_k^-	f_k^-/f_k^+
			From Hirshfeld atomic charges					
O1	0.04371	0.12828	0.0063	0.03027	0.08884	0.00437	1.443894	0.692572
O2	0.02331	0.06839	0.00336	0.0397	0.11651	0.00572	0.587028	1.703497
O3	0.06084	0.17855	0.00877	0.1322	0.38797	0.01906	0.460222	2.172863
O4	0.06766	0.19855	0.00976	0.03654	0.10722	0.00527	1.851763	0.540026
N5	0.02175	0.06382	0.00314	0.01207	0.03543	0.00174	1.801441	0.555111
O6	0.05153	0.15123	0.00743	0.1272	0.3733	0.01834	0.405132	2.46833
N7	0.09185	0.26956	0.01324	0.01662	0.04878	0.0024	5.525597	0.180976
N8	0.06127	0.17981	0.00883	0.0805	0.23625	0.01161	0.761084	1.313916
C9	0.01669	0.04897	0.00241	0.00821	0.0241	0.00118	2.031905	0.492149
C12	0.01058	0.03104	0.00153	0.01044	0.03065	0.00151	1.012735	0.987426
C13	0.08536	0.25051	0.01231	0.04099	0.12028	0.00591	2.082689	0.480149
N14	0.01272	0.03732	0.00183	0.07236	0.21235	0.01043	0.175751	5.689864
C15	0.04693	0.13774	0.00677	0.05987	0.1757	0.00863	0.783941	1.275606
C16	0.02353	0.06905	0.00339	0.02403	0.07051	0.00346	0.97919	1.021252
C17	0.06122	0.17968	0.00883	0.05015	0.14717	0.00723	1.220915	0.819058
C19	0.08839	0.2594	0.01274	0.04709	0.13819	0.00679	1.877161	0.532719
C21	0.04638	0.13612	0.00669	0.06503	0.19085	0.00938	0.713218	1.402096
N24	0.00414	0.01214	0.0006	0.00305	0.00896	0.00044	1.354406	0.738331
O25	0.0049	0.01437	0.00071	0.00368	0.01079	0.00053	1.331702	0.750919

C26	−0.0046	−0.0134	−0.0007	−0.0039	−0.0113	−0.0006	1.183965	0.84462
O27	−0.0097	−0.0285	−0.0014	−0.0085	−0.0249	−0.0012	1.148135	0.870978
C28	−0.0007	−0.002	−1E−04	−0.001	−0.0028	−0.0001	0.708247	1.411936
C30	0.00924	0.0271	0.00133	0.00715	0.02097	0.00103	1.292512	0.773687
C32	0.00612	0.01797	0.00088	0.00495	0.01454	0.00071	1.236422	0.808785
C34	0.00214	0.00627	0.00031	0.00183	0.00536	0.00026	1.170318	0.854469
C35	0.00193	0.00568	0.00028	0.00133	0.00391	0.00019	1.451952	0.688728
C37	0.00363	0.01064	0.00052	0.00271	0.00794	0.00039	1.340481	0.746001